

# Optimal Processing and Performance Evaluation of Passive Acoustic Systems

by

Peter Lawrence Greene

Submitted to the Department of Electrical Engineering and  
Computer Science  
in partial fulfillment of the requirements for the degree of  
Master of Engineering in Electrical Engineering and Computer  
Science


at the

MASSACHUSETTS INSTITUTE OF TECHNOLOGY

June 1997

© Peter Lawrence Greene, MCMXCVII. All rights reserved.

The author hereby grants to MIT permission to reproduce and  
distribute publicly paper and electronic copies of this thesis  
document in whole or in part, and to grant others the right to do so.

Author  .....  
Department of Electrical Engineering and Computer Science  
23 May 1997

OCT 23 1997

Certified by  .....  
Dr. Thomas J. Green, Jr.  
Technical Staff, Lincoln Laboratory  
Thesis Supervisor

Accepted by  .....  
Arthur C. Smith  
Chairman, Departmental Committee on Graduate Students

# Optimal Processing and Performance Evaluation of Passive Acoustic Systems

by

Peter Lawrence Greene

Submitted to the Department of Electrical Engineering and Computer Science  
on 23 May 1997, in partial fulfillment of the  
requirements for the degree of  
Master of Engineering in Electrical Engineering and Computer Science

## **Abstract**

Modern research in the field of underwater acoustics is aimed at developing automated target recognition and identification systems. This thesis develops the optimal detector for a certain class of underwater signals and analyzes the effect that different estimation attributes have on detection. Development of the optimal detector will contribute insight into optimizing practical processors as well as provide benchmarks to measure performance of such processors.

Thesis Supervisor: Dr. Thomas J. Green, Jr.  
Title: Technical Staff, Lincoln Laboratory

## Acknowledgments

I humbly offer my thanks to the Lord God and his son, Jesus Christ. I have truly been blessed with my family, friends and opportunities thus far in my life, and I am grateful for the gifts that enabled me to complete this thesis.

I salute my parents, Robert and Peggy Greene, for teaching me so much that could never be taught in any institution. I also thank them for the support, both emotionally and financially, that allowed me to pursue my education these last five years of my life. I also salute my grandparents and all they have done for me and continue to do for me every day.

There are many instrumental people, without whom my thesis would have completely fallen apart, the most significant of these being my thesis advisor, Dr. Thomas Green, Jr. I can honestly and sincerely say, that Tom, along with many other Lincoln Lab employees, taught me more in this last year than I learned in any of my four previous years at MIT. Tom taught me things intellectually, spiritually, emotionally and basketbally, that I never dreamed I would learn while working on my thesis. Thanks Tom, for everything, God bless him, his wife Elizabeth and his son Matthew.

Another person instrumental in my thesis experience is my mentor and friend, Lieutenant Matthew Kosnar, USN. Without Matt's help, I never would have had the chance to participate in the little-known Navy program that allowed me to finish this fifth year in the first place. Matt has also been a wealth of knowledge for me and is often the first person I look to for advice. Matt helped inspire me to finish my Masters, learn guitar, love to sail and to join him and the ranks of honorable men in the United States Navy submarine community.

I must also sincerely thank the United States Navy for the great opportunity it has allowed me to pursue here at MIT. I eagerly await the day when I may serve my country as well as it has me. Thanks also to the United States Air Force for the respect and generosity they have shown me as I researched my thesis on Hanscom AFB. Thanks also to my superior, Lieutenant Commander Mark Welsh, USN, and Richard Galione for their help during my graduate year at MIT.

I offer my sincere thanks to MIT, the staff of the Electrical Engineering department and especially my academic advisor, Professor Jeffrey Shapiro.

I have to thank everyone at Lincoln Laboratories for help on countless points of my thesis. They include: Dr. Richard Lacoss and Dr. Paul Kolodzy for the opportunity to work at Lincoln as well as their assistance with my thesis, Jerry Baum, Carol Lazott, Vivian Titus, Rob Baxter, Dr. Dan Dudgeon, Dr. Tom Quatieri, Bill Payne and Dr. Vincent Premus for everything from probability theory to yelling “stupid, stupid, stupid...” at my computer, and Eric Van Allen and Dave Ireland for the stress relief they brought me.

Lastly, I offer the crew of the USS Whale (SSN 638) my thanks for combining my academic interests and career goals and inspiring me to enjoy it to the fullest.

The research for this thesis was supported in part by the U. S. Navy Space and Naval Warfare Systems Command (SPAWAR).

# Contents

<b>1</b>	<b>Introduction</b>	<b>11</b>
1.1	Passive Acoustic Sensing . . . . .	11
<b>2</b>	<b>Bin Statistics</b>	<b>13</b>
2.1	Lofargram . . . . .	13
2.2	Single Pixel Density Function . . . . .	15
2.2.1	Exponential Bin Statistics . . . . .	16
2.3	Experimental Verification . . . . .	16
2.4	Deviation From Exponential . . . . .	17
<b>3</b>	<b>Target Detection Theory</b>	<b>22</b>
3.1	Binary Hypothesis Testing and the LRT . . . . .	22
3.1.1	Detection, False Alarm and Miss Probabilities . . . . .	24
3.1.2	Neyman-Pearson Optimal Detector . . . . .	25
3.2	Unknown Parameters (GLRT) . . . . .	25
3.3	Performance Assessment and Terminology . . . . .	26
<b>4</b>	<b>Background and Signal Modeling</b>	<b>28</b>
4.1	Signal Modeling . . . . .	30
4.2	Background . . . . .	34
4.2.1	Ambient-Noise . . . . .	34
4.2.2	Biologics . . . . .	36
4.2.3	Background Examples . . . . .	36

4.2.4	Clutter . . . . .	36
<b>5</b>	<b>Optimal Processing</b>	<b>39</b>
5.1	Signal and Background Density Functions . . . . .	39
5.2	LRT Derivation . . . . .	40
<b>6</b>	<b>Performance Assessment</b>	<b>44</b>
6.1	Performance Metrics Throughout the Detection Process . . . . .	45
6.1.1	Phone Level Signal-to-Noise Ratio . . . . .	45
6.1.2	Ratio of Bandlimited Energies . . . . .	46
6.1.3	Output Signal-to-Noise Ratio . . . . .	46
6.2	A Simple Example . . . . .	47
6.3	Performance Bounds . . . . .	49
6.3.1	Chernoff Bound Approximation . . . . .	49
6.3.2	Error Function Approximation . . . . .	50
6.3.3	Simulation Analysis . . . . .	51
<b>7</b>	<b>LRT and EBD Analysis</b>	<b>52</b>
7.1	Number of Feature Regions Utilized . . . . .	52
7.2	LRT versus EBD . . . . .	56
7.3	The Non-Ideal EBD and Signal-Like Clutter . . . . .	58
<b>8</b>	<b>Background Estimators</b>	<b>62</b>
8.1	NSE . . . . .	62
8.2	Optimizing the Three-Pass NSE . . . . .	64
8.2.1	Optimal Gate Width . . . . .	64
8.2.2	Optimal Smoothing Window Length . . . . .	66
8.2.3	Optimal Threshold . . . . .	68
8.2.4	NSE Parameter Setting Summary . . . . .	72
8.3	Comparison of NSE Parameters . . . . .	72
<b>9</b>	<b>Evaluation of Background Estimators</b>	<b>74</b>

9.1 Data Generation . . . . .	74
9.2 Detector Performance Results . . . . .	75
<b>10 Conclusions</b>	<b>79</b>
<b>A Exponential Bin Statistics Derivation</b>	<b>81</b>

# List of Figures

2-1	Bin Statistics Processing Diagram . . . . .	14
2-2	The Axes of a Waterfall Display . . . . .	15
2-3	A Gram Excerpt Containing Data Distributed Exponentially . . . . .	18
2-4	Histogram of Exponential Bin Statistics . . . . .	18
2-5	A Gram Excerpt Containing Data Distributed Other Than Exponentially . . . . .	19
2-6	Histogram of Other Than Exponential Bin Statistics . . . . .	20
3-1	Binary Hypothesis Distribution . . . . .	23
4-1	Frequency Bins or Pickets (k) and Feature Regions (m) . . . . .	29
4-2	Inbands plus Broadband of Spectral Density Average . . . . .	30
4-3	Inbands of Spectral Density Average . . . . .	31
4-4	Simple Signal Model . . . . .	33
4-5	Average deep-water ambient-noise spectra . . . . .	35
4-6	Noise spectra at coastal locations with wind speed as a parameter . . . . .	35
4-7	White Noise Gram and corresponding Amplitude Scan (ASCAN) . . . . .	37
4-8	Non-Quiescent Gram and ASCAN . . . . .	37
6-1	PLSNR, RBLE & SNRO . . . . .	45
6-2	Error Function, Simulation and Chernoff Boundries . . . . .	51
7-1	$J/M$ Versus Loss Factor $\epsilon(J, M)$ for EBD . . . . .	55
7-2	$c$ versus $P_F$ for various values of $P_C$ . . . . .	61
8-1	Noise Spectral Equilizer . . . . .	63



8-2	MSE vs. Gate Width . . . . .	65
8-3	Optimal Gate Width Over Largest Feature . . . . .	66
8-4	First pass clipping effect on signal feature . . . . .	67
8-5	Second Pass Window Length vs. MSE . . . . .	68
8-6	Optimal Threshold for Flat Background and Low SNR . . . . .	69
8-7	Optimal Threshold for Flat Background and Mid SNR . . . . .	70
8-8	Optimal Threshold for Flat Background and High SNR . . . . .	71
9-1	Synthetic Signal and Synthetic Background, PLSNR = $-23.42\text{dB}$ . .	76
9-2	Synthetic Signal and Real Background, PLSNR = $-11.69\text{dB}$ . . . . .	77
9-3	Real Signal and Synthetic Background . . . . .	78
9-4	Real Signal and Real Background . . . . .	78

# List of Tables

8.1 Three-Pass NSE Parameters . . . . . 73

# Chapter 1

## Introduction

The signal processing behind modern passive acoustic sensing is continually improving automatic target recognition (ATR) capabilities. Current technology is aimed at providing a variety of information that assists the human sonar operator in making the decision as to whether or not a target has been located. ATR systems are being developed to detect and classify acoustic target signatures in a variety of background noise and clutter. Several systems have met with some success in target recognition; however, the ATR problem is far from solved. This thesis focuses primarily on developing, through detection theory, a detection bound referred to as *optimal performance*. With these bounds, it is hoped that the validity of practical ATR processors can be assessed in the research laboratory.

### 1.1 Passive Acoustic Sensing

Acoustic energy has long been a useful source for underwater detection and classification. This is due partly to the excellent acoustic transmission properties of seawater and the relative lack of other means by which to detect underwater targets. Acoustic sensing is possible through both actively searching and passively listening to the ocean environment. Passive sensing is appealing because it emits no detectable energy and thereby one does not compromise one's position to learn the location of another platform. All acoustic sensing makes use of microphones and transducers to detect

acoustic energy and convert it to an electrical signal. Hydrophones, or underwater microphones, are used to receive acoustic data from the ocean and to transform it to electric energy. Typically arrays of hydrophones are used in order to improve the signal-to-noise ratio (SNR) and to help define the acoustic energy source's direction through phase differences of received signals (beamforming) [9]. Passive acoustic detection is the ability to detect these signals above the noise of naturally occurring acoustic energy in the ocean.

The remainder of this thesis is organized as follows: Chapter 2 presents the statistics of underwater signals, gives the assumptions presumed for this thesis and discusses any discrepancies. The theory behind binary hypothesis testing and optimal detection is explained in Chapter 3. The modeling of signals, background and clutter are discussed in detail in Chapter 4. Chapter 5 develops the optimal processor and evaluates its performance due to parameter variations. Using modeling information from Chapter 4, Chapter 6 develops signal-to-noise ratio (SNR) as a useful metric and discusses the relationship between various measurable SNRs. Chapter 7 is a closed form analysis of the likelihood-ratio test and other detectors. Chapter 8 explains the purpose behind background estimation and discusses optimizing one particular background estimation algorithm. The results computed from running the optimal detection algorithm under a variety of circumstances are compared and discussed in Chapter 9. Finally, Chapter 10 summarizes the major conclusions of this thesis.

# Chapter 2

## Bin Statistics

A collection of one or more acoustic radiators produces an acoustic field that can be detected by a hydrophone or hydrophone array. A hydrophone, or transducer, converts the acoustic energy into electrical energy that is processed by an anti-aliasing filter and digitized for further processing. Figure 2-1 depicts the process which converts raw ocean acoustic data into digital information, known as the acoustic time-series, to be processed by the detector. First, we assume that the raw ocean acoustic data is a zero-mean Gaussian random process (GRPZM)[1]. This data is low-pass filtered (LPF) and sampled by an analog-to-digital (A/D) converter, creating a series of discrete Gaussian random variables. These Gaussian random variables are further processed by a Discrete Fourier Transform (DFT), typically implemented with the Fast Fourier Transform (FFT) algorithm. The data now takes on the form of a complex Gaussian random process due to the FFT's transformation. Finally the magnitude-square is computed of each complex random variable, creating a discrete process consisting of exponential random variables (Appendix A).

### 2.1 Lofargram

The digital sequence  $x_i$  is known as the *time-series data* (see Figure 2-1). A sliding window depicts the portion of the data to be processed by the DFT. These non-overlapping windows are indexed by  $n$  and referred to as time epochs. After the

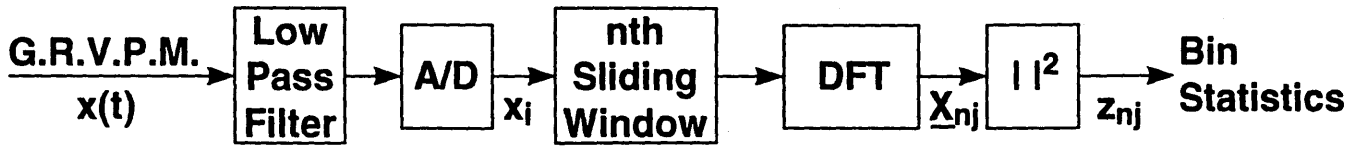


Figure 2-1: Bin Statistics Processing Diagram

DFT, the transformed time epoch is termed an individual scan line. Multiple scan lines compose a scan where  $X_{nj}$  is a way of representing the magnitude of each frequency bin  $j$  of the  $n^{\text{th}}$  scan line of the processed data. Finally,  $z_{nj}$  is the output of the magnitude squaring process, a function implemented to simplify the output statistics (Appendix A) and subsequent processing. In the following process,  $L$  is the number of samples of shift between adjacent scan lines and  $I$  is the number of samples used in the DFT. This squared-magnitude of a sliding time-windowed DFT is known as the low-frequency acoustic gram, the lofargram or simply the gram [3] and is given by<sup>1</sup>

$$z_{nj} \equiv \left| \sum_{i=0}^{I-1} x_{i+nL} e^{-j2\pi ij/I} \right|^2, \quad 0 \leq j \leq I/2 - 1. \quad (2.1)$$

The gram is a series of individual scan lines stacked one on top of another such that the x-axis is increasing frequency and the y-axis is decreasing time. This is commonly termed the *waterfall* display (Figure 2-2).

Each pixel on the waterfall display represents a particular frequency bin, for a particular scan line. The darkness of the pixel is proportional to the relative power present in that frequency bin. This shading is termed *gray-scaling*.

<sup>1</sup>Note the two  $j$ 's in the exponent of Equation 2.1. The first  $j$  corresponds to the imaginary value of  $\sqrt{-1}$  and the second  $j$  indexes the frequency picket.

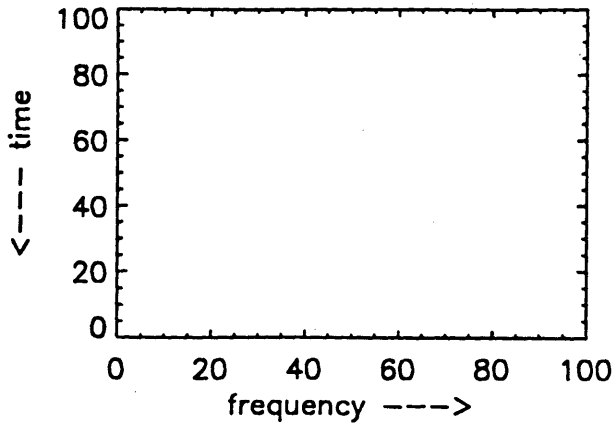


Figure 2-2: The Axes of a Waterfall Display

## 2.2 Single Pixel Density Function

It is important that we understand the distributions behind passive acoustic data because assumptions about the distributions shape the tools we use for detection and classification. For instance, we assume that underwater acoustic signals are stochastic, not deterministic processes. In addition, we assume that these stochastic processes are all Gaussian in nature. The simplification of the detector used in this thesis relies on these statistics. The degree to which our results are reliable directly relates to the degree to which our assumed stochastic processes accurately model the real world data. For example, if the statistical distributions are assumed to be Gaussian in nature, then knowing the first two moments will completely describe the process and allow us to construct a detector relying only on the values of the first and second moment, even if they vary with time. If, however, the pixels are distributed otherwise, we could be throwing away valuable information by ignoring the other moments, and performance could suffer.

Previous designs have indeed relied on the assumption that our particular signals of interest and typical ocean noise are zero-mean complex Gaussian random processes [1]. This thesis uses an optimal test, developed in Chapter 5, that is based on a

Gaussian assumption. The Gaussian statistics in time yield exponential statistics when working with magnitude-squared Fourier transforms in the gram domain.

### 2.2.1 Exponential Bin Statistics

The most practical place to measure real data statistics in the processing outlined in Figure 2-1 is immediately after the magnitude-square transformation, or where we construct the gram. It is important to verify the exponentiality of the statistics at this point in the processing, as this is the starting point for all detection and estimation. The magnitude squaring produces exponential statistics (Appendix A) which simplifies (Chapter 5) subsequent processing.

Previously we have stated our assumption that the input to our processing system is a Gaussian random process with zero mean. The low-pass filter and DFT generate complex random variables having independent Gaussian real and imaginary components with zero means and identical variances. The FFT implementation of the DFT is a linear transform explained in detail in most discrete-time signal processing books [5] which generates the same independent complex Gaussian components as mentioned for the DFT process. The independent Gaussian random variables of the zero-mean complex random process are effectively transformed into exponential random variables by the non-linear magnitude-squared process that produces the gram. The math that yields these exponential random variables is included in Appendix A.

## 2.3 Experimental Verification

It has been shown that prior assumptions about the statistical distributions of acoustic ocean data would yield exponential distributions under stationary<sup>2</sup> means. There are, however, several examples of real data under stationary environments that yield distributions differing from an exponential curve. This section will show that under

---

<sup>2</sup>Since it is cumbersome for the author to determine wide-sense stationarity analytically, this is *assumed* stationarity where the gram appears to have a relatively constant mean, a necessary but not sufficient condition.



most circumstances we can generate a histogram of background statistics which corresponds well with an exponential distribution, but that it is also possible to locate background statistics which deviate from an exponential distribution.

It is possible to create a histogram of the statistics associated with a particular frequency bin over several scan lines. We divide all bins by their respective averages to create a histogram over both multiple time scans and multiple frequency bins. Specifically, we want to generate a histogram of the normalized gram,  $\tilde{z}_{nj}$ ,

$$\tilde{z}_{nj} = \frac{z_{nj}}{\frac{1}{N} \sum_n z_{nj}}. \quad (2.2)$$

We normalize each frequency bin to a unity mean and variance<sup>3</sup> over all time epochs because the different bins, although assumed exponential, do not necessarily have the same mean and variance. In this manner we can process real ocean acoustic data to evaluate the assumptions that lie behind our statistics. Figure 2-3 is a lofargram of ocean noise which matches well with an exponential curve in Figure 2-4. These results are typical of much real noise that the author processed.

The straight line generated in Figure 2-4 is simply the best fit exponential curve plotted on the logarithmic plot. This same curve could be found analytically by measuring the mean value of the statistics and then plotting the function  $x(t) = \frac{1}{\lambda} e^{-\frac{t}{\lambda}}$  where  $1/\lambda$  is the measured mean and  $x(t)$  the normalized number in each bin  $t$ .

## 2.4 Deviation From Exponential

Figure 2-5 and Figure 2-6 are the lofargram of deviant statistics and its corresponding histogram. The author has found these statistical variations to be prevalent in *dark* portions of the gram, or time-frequency spaces with large amounts of energy. The dark strip of the Figure 2-5 gram excerpt is the section analyzed in order to produce the related histogram. The author was careful to include only the middle regions of the

---

<sup>3</sup>Note that dividing by the mean normalizes the assumed exponential statistics, but does not necessarily normalize non-exponential statistics.

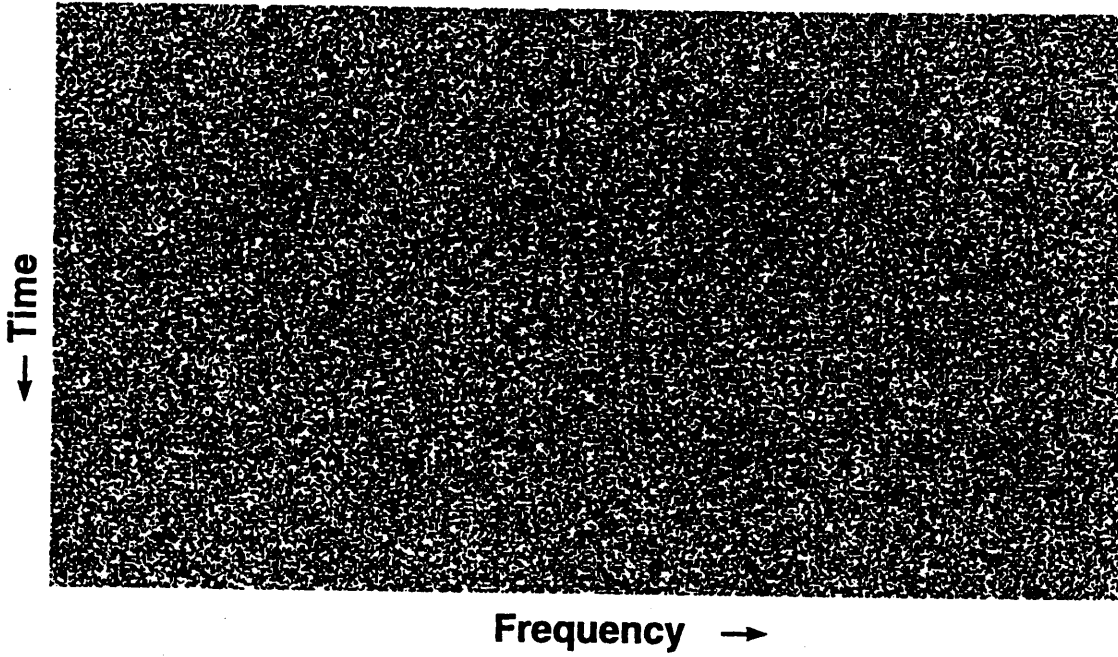


Figure 2-3: A Gram Excerpt Containing Data Distributed Exponentially

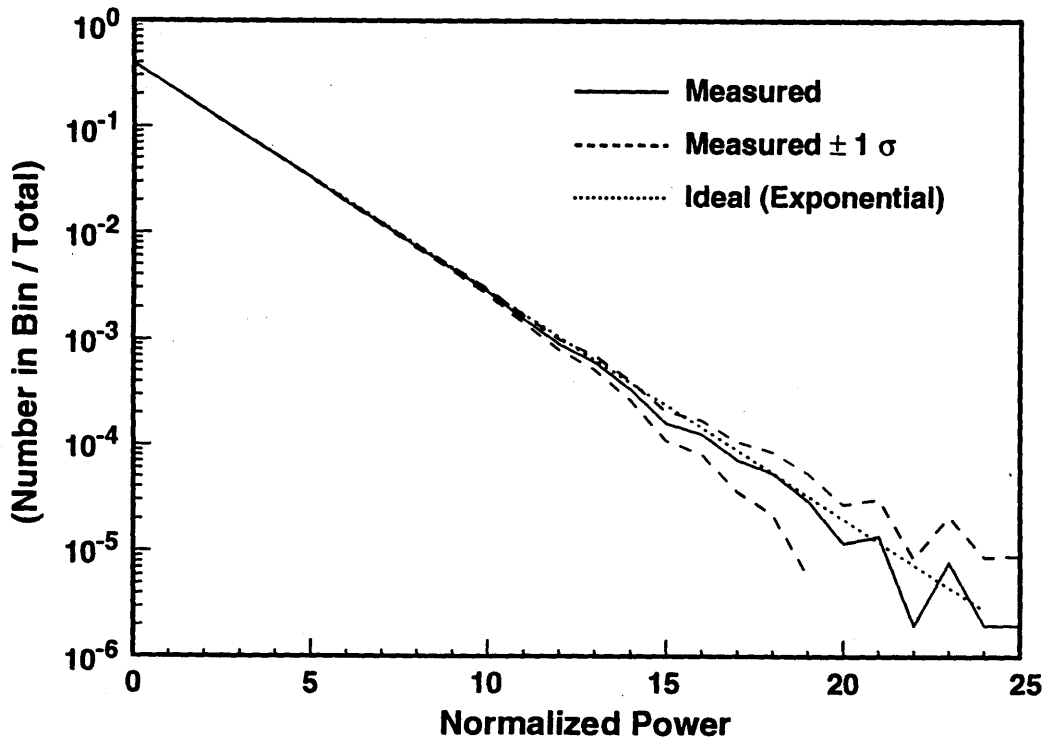


Figure 2-4: Histogram of Exponential Bin Statistics

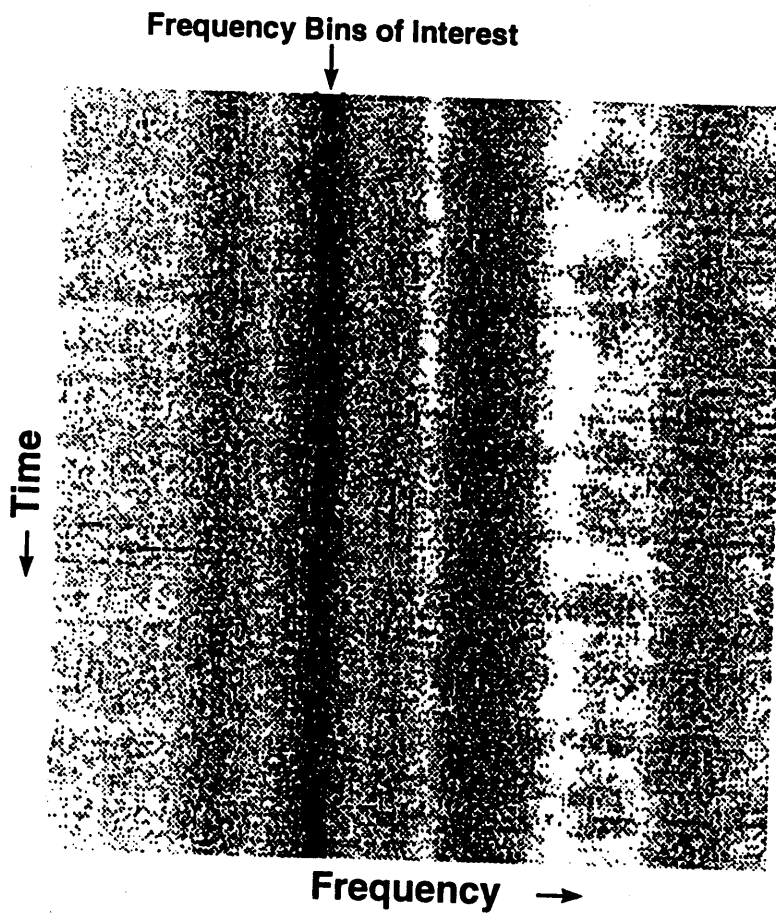


Figure 2-5: A Gram Excerpt Containing Data Distributed Other Than Exponentially

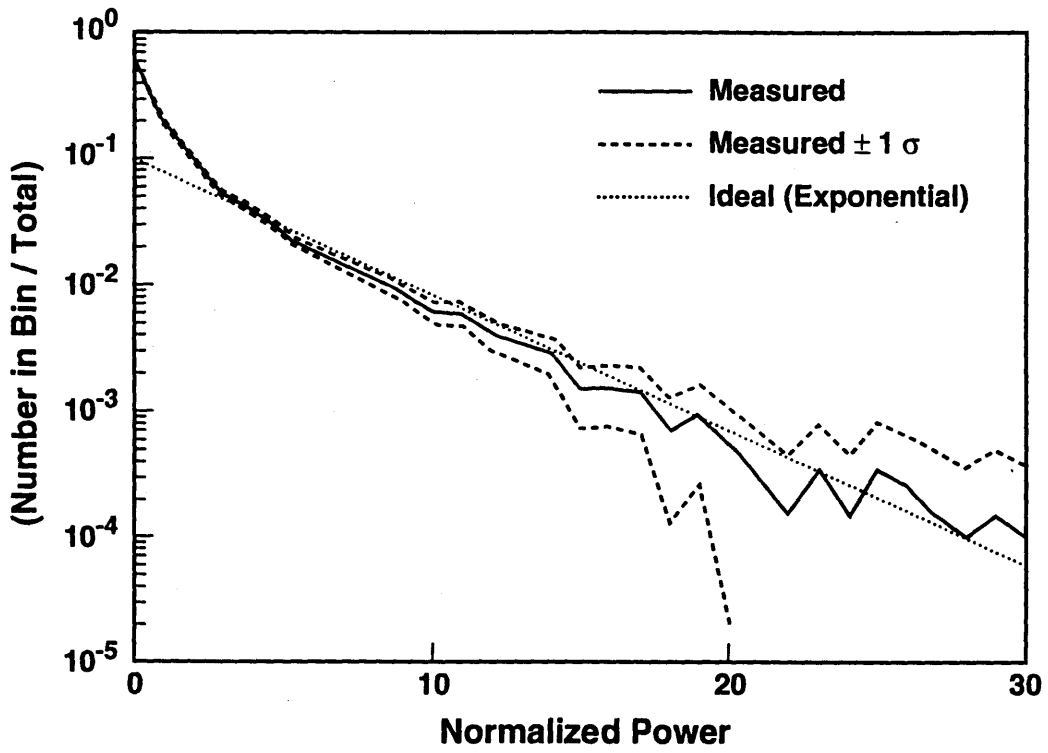


Figure 2-6: Histogram of Other Than Exponential Bin Statistics

dark spots in order to preserve what sense of stationarity exists. This deviation from the exponential distribution, although much less common, is still prevalent in ocean noise. The histograms include error plots for plus or minus one standard deviation to lend validity to the plot. The deviant data was collected from a single-element sonabouy in a deep-water environment.

In Figure 2-6 it is obvious that even the best-fit exponential curve does not well model the background statistics. If an exponential were drawn with the same mean as the deviant background statistics, it would match well with the more frequently occurring normalized power bins, but would fall well below the occurances in bins farthest from the mean. These distant bins are referred to as *tails* in the distribution.

There are a few theories that could explain the exponential tails exhibited in Figure 2-6. The tails could be due to a non-stationary (time-varying mean) background, or to the presence of transients in strong signals. Transients are short duration strong signals that begin to look like an impulse in time to the receiver. The Fourier transform of the impulse is a flat white noise spectrum. This high-amplitude scan line in the spectrogram is typically several standard deviations greater than the expected value of the bins in that scan line. Consequently, a histogram will exhibit these abnormally deviant bins as tails in the exponential distribution.

Close examination of the distribution will show that there are more occurances of large values as compared to the exponential distribution. Since the histogram necessarily integrates to the same area under both plots, it is easily seen that having a greater number of occurances several standard deviations away will cause a corresponding decrease in the number of occurances close to the mean.

Even if transients or non-stationarity are not responsible for the abnormalities in the statistics, let it suffice that this thesis has shown there is some deviation for strong sources. Although this deviation occurs with less frequency than the distributions more closely associated with the exponential distribution, it is important that we recognize that it exists and may affect our detector. However, for the remainder of this thesis, we will assume that we are working only with ocean data that is adequately modeled by exponential spectral statistics.

# Chapter 3

## Target Detection Theory

A classic component of basic target detection and a vital part of passive acoustic sensing is binary hypothesis testing. This chapter presents the optimal detector and the basic detection theory necessary to understand it. We also describe several tools to help assess the performance of a given detector.

### 3.1 Binary Hypothesis Testing and the LRT

The two hypotheses used in binary target detection are  $H_1$  or “target present” and  $H_0$  or “target absent”. Our challenge is to make the best decision with the given information between mutually exclusive hypotheses. Consider a data vector  $\underline{z}_n$  that has the following distributions,

$$\begin{aligned} H_0 & : p_{\underline{z}_n|H}(\underline{z}_n|H_0) \\ H_1 & : p_{\underline{z}_n|H}(\underline{z}_n|H_1), \end{aligned}$$

where

$$\underline{z}_n = [z_{n1} \ z_{n2} \ z_{n3} \ \cdots \ z_{nI/2}]^T.$$

The likelihood ratio test (LRT) is a comparison of the ratio of probability distri-

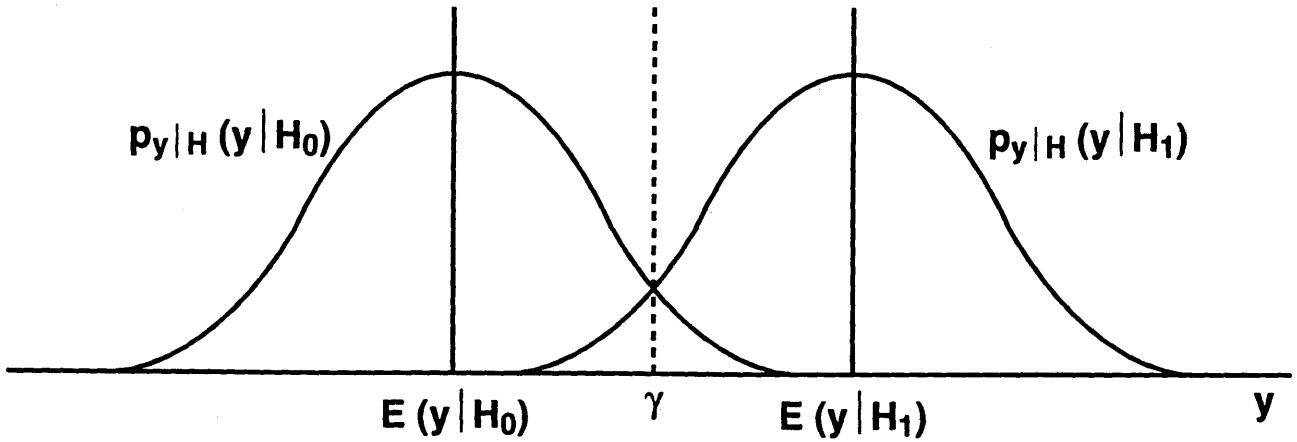


Figure 3-1: Binary Hypothesis Distribution

butions of our data vector  $z_n$  compared to a threshold  $\gamma$ . Based on this comparison we map each  $z_n$  to a particular hypothesis. We write the LRT as

$$L(z) \triangleq \frac{p_{z_n|H_1}(z_n|H_1)}{p_{z_n|H_0}(z_n|H_0)} \underset{\hat{H}(z_n)=H_0}{\overset{\hat{H}(z_n)=H_1}{\geq}} \frac{P_0(C_{10} - C_{00})}{P_1(C_{01} - C_{11})} \triangleq \gamma. \quad (3.1)$$

$\hat{H}(z_n)$  is a mathematical function which maps each  $z_n$  to hypothesis  $H_1$  or  $H_0$ .  $C_{xy}$  is the cost of choosing  $H_x$  when in fact  $H_y$  is true. If we set  $C_{00} = C_{11} = 0$  and  $C_{10} = C_{01} = 1$  we achieve the minimum probability-of-error (MPE) criterion. In addition, setting  $P_0 = P_1$  achieves the maximum likelihood (ML) decision rule.

It is important to note that  $L(z)$  (herein referred to as the detection metric  $y$ ) is a *sufficient statistic*. By this we mean that everything we need to know about the observation vector  $z_n$  in order to make the best or *optimal*, in a minimum average cost sense, decision is contained in  $y$ .

Chapter 5 will show that based on our Gaussian input assumption, the detection metric  $y$  is a sum of  $n$  non-Gaussian random variables. Let us assume that  $n$  is large enough so that the detection metric  $y$  appears Gaussian because of the Central Limit

Theorem. This being the case,  $y$  takes on the distributions

$$\begin{aligned} H_0 &: p_{y|H}(y|H_0) \\ H_1 &: p_{y|H}(y|H_1), \end{aligned}$$

as depicted in Figure 3-1. Note also the threshold  $\gamma$  which allows us to define the detection probabilities.

### 3.1.1 Detection, False Alarm and Miss Probabilities

The detection, false alarm and miss probabilities are useful metrics for measuring the relative performance of different processors. The probability of detection ( $P_D$ ) is the chance that  $y \geq \gamma$  given  $H = H_1$  where  $\gamma$  is a detection threshold chosen to achieve a particular performance

$$P_D = \int_{\gamma}^{\infty} p_{y|H}(y|H_1)dy. \quad (3.2)$$

The probability of false alarm ( $P_F$ ) is the chance that  $y \geq \gamma$  given  $H = H_0$

$$P_F = \int_{\gamma}^{\infty} p_{y|H}(y|H_0)dy. \quad (3.3)$$

Note that increasing the detection threshold will lower the chance that we “say” there is a target present when there is not ( $P_F$ ). However, raising the threshold also decreases the probability that we recognize a target when it is present. Varying  $\gamma$  is simply a trade off between  $P_F$  and  $P_D$ , so often we will adjust  $\gamma$  such that we have a particular false alarm (i.e.  $P_F = 10^{-3}$ ) and then we can compare the  $P_D$  for each  $\underline{z}_n$  and the associated metric  $y$ . Note that the ML and MPE criterion set the threshold and therefore dictate the  $(P_F, P_D)$  point at which to operate, however, the following section will present a test that allows us to choose a threshold value.

Finally, the probability of a miss ( $P_M$ ) is the chance that  $y < \gamma$  given  $H = H_1$

$$P_M = \int_{-\infty}^{\gamma} p_{y|H}(y|H_1)dy = 1 - P_D. \quad (3.4)$$



The miss probability is the chance that we will declare that no target is present when, in fact, there is a target present. Note that the miss and detection probabilities sum to one.

### 3.1.2 Neyman-Pearson Optimal Detector

Assigning the *a priori* probabilities of a target's presence or the costs associated with choosing a particular  $H_x$  is difficult for target detection. Therefore we will choose a threshold value based on the Neyman-Pearson criterion. The Neyman-Pearson optimality criterion maximizes  $P_D$  under the constraint that  $P_F = \alpha' \leq \alpha$  for any  $\alpha$  between 0 and 1 [11]. The likelihood-ratio test is the Neyman-Pearson optimal detector with a threshold,  $\gamma$ , that meets the optimality criterion.

A commonly used threshold value is three times the standard deviation of the null hypothesis, or  $3\sigma$ . This  $3\sigma$  is approximately equivalent to setting  $P_F = 10^{-3}$  under the constraint that the distribution of the detection metric is Gaussian and that maximizing  $P_F$  maximizes  $P_D$ .

## 3.2 Unknown Parameters (GLRT)

The application of the Neyman-Pearson optimal detector to real passive acoustic data requires some adjustment. The PDF for any particular target varies with range, depth, environment and a multitude of other factors too numerous to count. The background noise in an underwater ocean environment varies with numerous factors as well and is less predictable than even the target. In order to utilize the optimal decision criterion outlined above, we must make estimates of both the  $H_0$  and the  $H_1$  PDFs. This leads to a generalized LRT in place of the LRT, which employs a LRT with ML estimates. However, we will look at various estimation techniques for unknown parameters and utilize a quasi-GLRT (henceforth referred to as GLRT) to see how these different estimates affect detector performance.

### 3.3 Performance Assessment and Terminology

There exist many tools to analyze the performance of various components of the detector. One such tool is the *deflection characteristic* ( $d$ ),

$$d \triangleq \frac{[E(y | H_1) - E(y | H_0)]^2}{\text{var}(y | H_0)}. \quad (3.5)$$

Deflection is a measure of the difference in expected values between  $H_0$  and  $H_1$  over the standard deviation of  $H_0$ . A second tool is signal-to-noise ratio (SNR), given by:

$$\text{SNR} \triangleq \frac{\text{Average Signal Power}}{\text{Average Noise Power}} \triangleq \frac{E(z|\hat{H} = H_1) - E(z|\hat{H} = H_0)}{E(z|\hat{H} = H_0)}. \quad (3.6)$$

Both  $d$  and SNR can be defined at various points in the processing chain. We will look at meaningful measurements of these values in Chapter 5 and explore the relationships between these quantities and detection performance.

There are several terms which are intimately related with detection theory. They are false alarm rate, minimum detectable level, time-to-detect and hold-time-ratio. False alarm rate (FAR), e.g. alerts per hour, is the rate at which the detector produces a false alarm. We can raise the FAR by lowering our threshold,  $\gamma$ , and vice-versa. There is a trade-off between lowering the threshold in order to increase  $P_D$  and raising it to keep the FAR at a level reasonable for a sonar operator to track every false alarm and realize that it is in fact a false alarm. FAR is a measure of operator workload.

Minimum detectable level (MDL) depicts the lowest SNR for a given  $\{P_F, P_D\}$  that is considered a detection by the sonar operator. MDL is a measure of system sensitivity to weak signals. Common values of  $P_D$  and  $P_F$  at the MDL are 0.5 and  $10^{-3}$  respectively.

Other performance considerations are the time-to-detect (TTD) and hold-time-ratio (HTR). TTD is the time-delay between the appearance of a target and a valid algorithm alarm and is related to the integration time needed when a target is present to register a “hit” or target present. TTD quantifies system latency.

HTR depicts the fraction of the time a target is present that the detector produces

an alarm. For a constant SNR target, the definition for HTR is identical to our definition of  $P_D$ . HTR is frequently used when comparing processing algorithms where the target SNR varies over the period of time the target is present.

While FAR, MDL, TTD and HTR are all important metrics for a practical detection system assessment, they are all related to the prime metrics  $P_F, P_D$ , deflection and signal-to-noise ratio. Thus, in the remainder of this thesis, we will focus on the prime metrics to assess system performance.

Now that we have developed the framework essential to target detection, we will describe the models assumed for this thesis and develop the theoretically optimal detector based on these assumptions.

# Chapter 4

## Background and Signal Modeling

Now that we have examined the statistics of ocean noise and outlined the detection theory used in this thesis, we shall develop models for background and target power spectral densities (PSDs). These models incorporate PSD feature regions of varying strengths, shapes and bandwidths. Figure 4-1 demonstrates three feature regions of various widths and strengths for a generic model. This chapter will adopt notation for and establish the importance of feature regions.

For the purpose of this thesis we define three distinct categories of bandwidths: broadband, narrowband and midband. Broadband features are single PSD features whose frequency bandwidth extends more than approximately twenty-five percent of the spectrum. Narrowband features are often only a few bins wide and extend no more than one percent of the spectrum. Midband falls in-between broadband and narrowband, it covers from approximately one percent to twenty-five percent of the spectrum, and describes the bandwidth of our selected feature regions.

Narrowband signal detection has been treated extensively in [4]. This thesis will concentrate on distinguishing midband signal features embedded in broadband noise features, referred to as background.

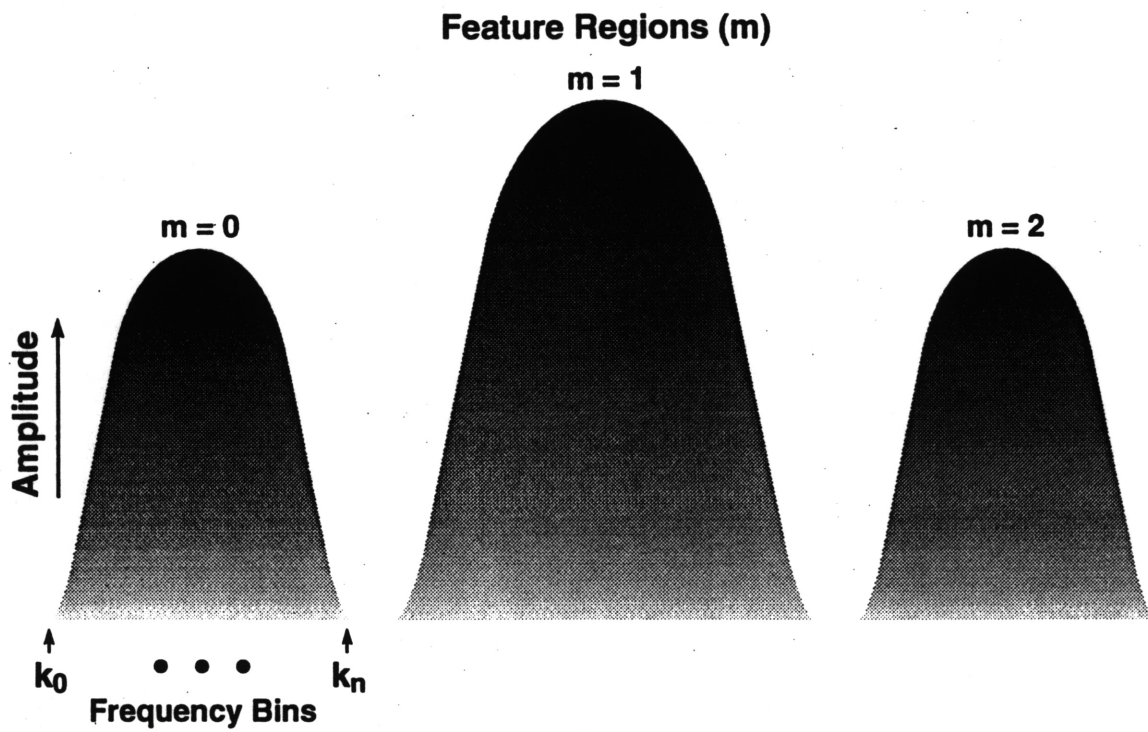


Figure 4-1: Frequency Bins or Pickets ( $k$ ) and Feature Regions ( $m$ )

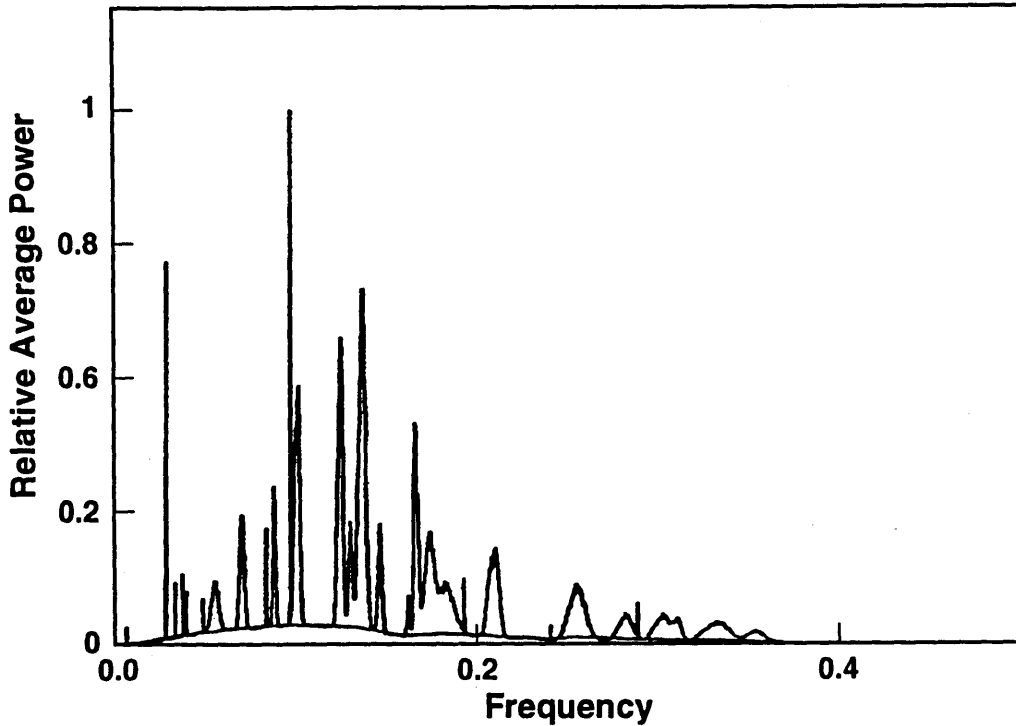


Figure 4-2: Inbands plus Broadband of Spectral Density Average

## 4.1 Signal Modeling

We are primarily concerned with detecting midband components of target signatures, although targets may exhibit narrowband and broadband components as well. A typical amplitude-scan (ASCAN) of a signal model is shown in Figure 4-2. The ASCAN is simply a time-averaged scan line,

$$\beta_j \equiv \frac{1}{N} \sum_{n=0}^{N-1} z_{nj}. \quad (4.1)$$

Note the difference between the relatively flat broadband ASCAN component and the midband-sized signal features on top of the broadband. We will refer to the midband-sized signal features here as *inbands*, which are extracted and shown alone in Figure 4-3. These inbands are analogous to the common barcode that labels most present-day consumer products. These barcodes have approximately 20–30 lines of varying widths printed with different spacing between every two lines. Laser scanners

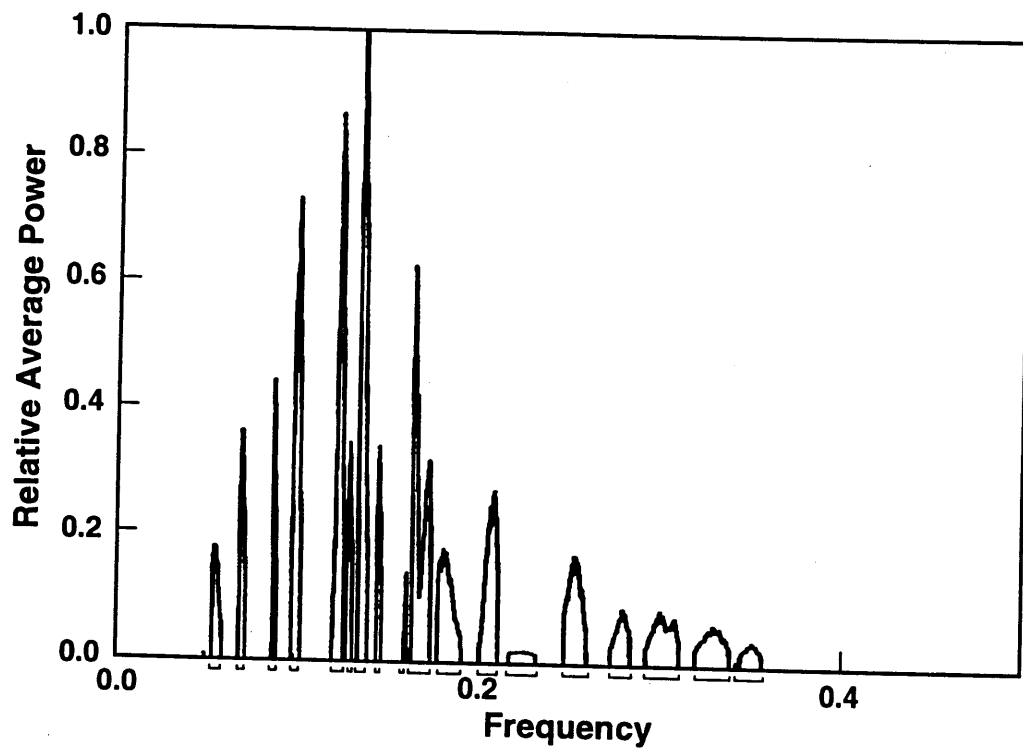


Figure 4-3: Inbands of Spectral Density Average

compare the reflection from these barcodes to a library of templates until it can match a template to the product being scanned. Similarly, we will take the magnitude-squared DFT processed data,  $z_{nj}$  and compare it to our library of target templates in hopes of matching two sets of inbands.

The feature regions alluded to in the introduction are simply midbands extracted from the vector  $\underline{z}_n$  of Chapter 2. The scan lines are still indexed by  $n$ , however, the frequency bin index is transformed so  $j = j_m + k$ ,

$$z_{nk}^m \equiv z_{n(j_m+k)}, \quad j_m + K_m \leq j_{m+1}.$$

Note that there are  $M$  feature regions, indexed by  $m$ , beginning with frequency bin  $j_m$ . Also, each feature region has  $K_m$  total bins indexed by  $k$ .

Let us choose a mean background  $\{\mu_k^m : 0 \leq m \leq M - 1, 0 \leq k \leq K_m - 1, \}$  such that it describes each bin  $k$  of each feature region  $m$  (see Figure 4-1). Note that these defined feature regions are *signal* feature regions. Later in this thesis it will be shown that optimal processing mandates a background model only for bins containing signal. This background model becomes the expected value of the processed DFT,  $z_{nk}^m$ , under the null hypothesis

$$E(z_{nk}^m | H_0) = \mu_k^m. \quad (4.2)$$

We will incorporate our signal model information into three parameter types:  $\alpha$ ,  $\lambda_k^m$ , and  $\phi_m$ ; where  $\alpha$  is the factor which scales the feature shape  $\lambda_k^m$  and strength  $\phi_m$ . The expected value of the DFT,  $z_{nk}^m$ , under the target present hypothesis is the sum of the uncorrelated background and signal means

$$E(z_{nk}^m | H_1) = \mu_k^m + \alpha \phi_m \lambda_k^m \quad (4.3)$$

where

$$\sum_{k=0}^{K_m-1} \lambda_k^m = 1, \quad 0 \leq m \leq M - 1,$$



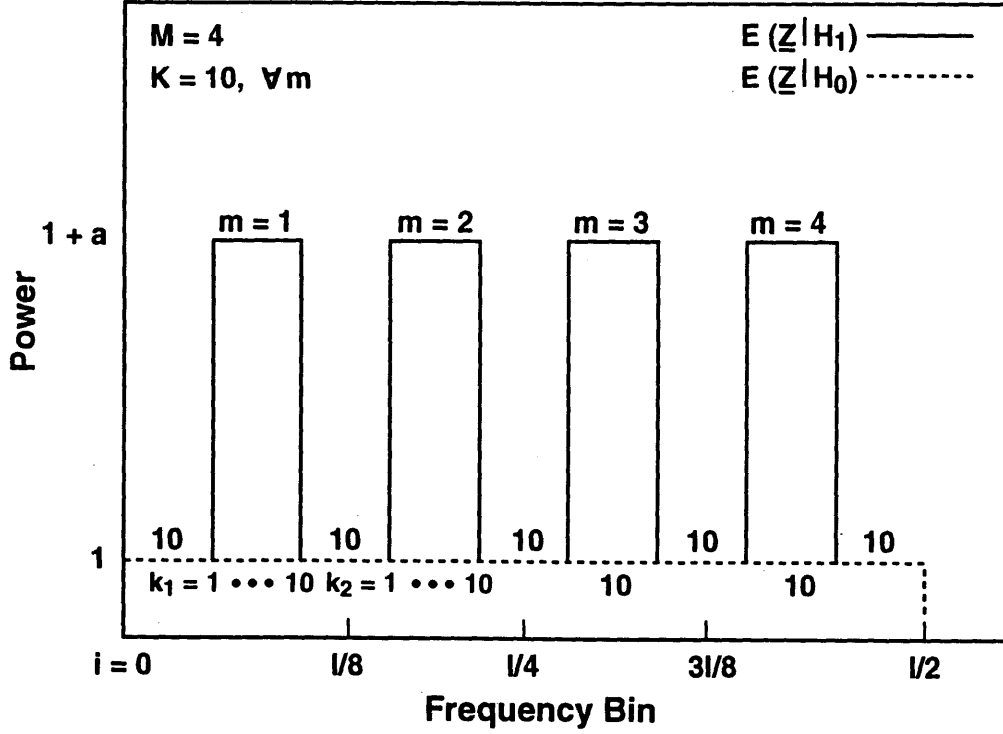


Figure 4-4: Simple Signal Model

$$\sum_{m=0}^{M-1} \phi_m = 1.$$

These normalizations allow us to specify the average bin-level signal strength as  $\alpha$  for all the feature regions.

Figure 4-4 is a simple model which incorporates  $M$  feature regions with  $K$  bins each, given by:

$$\begin{aligned} K_m &= K & \text{for } 0 \leq m \leq M-1, \\ \lambda_k^m &= \frac{1}{K} & \text{for } 0 \leq m \leq M-1, 0 \leq k \leq K_m-1 \\ \phi_m &= \frac{1}{M} & \text{for } 0 \leq m \leq M-1, \\ \alpha &= aKM & \text{and,} \\ \mu_k^m &= 1 & \text{for } 0 \leq m \leq M-1, 0 \leq k \leq K_m-1. \end{aligned}$$

The scaling factor  $\alpha$  and constant  $\lambda_k^m$  and  $\phi_m$  yield a signal strength of  $a$  in each bin. We utilize a flat background of strength one, thus the peak feature strength lies at  $a + 1$ . We will use this model and variations of this model in subsequent chapters for analysis purposes.

## 4.2 Background

It is instructive to divide background noise into two major categories, ambient and biologic noise, both of which can retard the ability to detect midband acoustic targets.

### 4.2.1 Ambient-Noise

Ambient-noise is generated by both man-made and naturally occurring sources. Natural noise can take many forms, like seaquakes, volcanoes, hydrostatic wave effects, ocean turbulence, non-linear wave interaction, thermal noise, ice breakage, rain, waves, tides and wind [9]. Some of these noise sources transmit acoustic signals that are received by the detecting hydrophone and other noise sources simply cause changes in sound speed (due to thermal and pressure variations) which, in turn, perturb signal frequencies, causing phase differences and statistical deviations which hinder detection. However, the most significant natural ambient noises are low frequency wavenoise and tidal currents (mostly  $< 10$  Hz,) and high frequency wind noise (mostly  $> 300$  Hz, see Figure 4-5) [9]. Man-made ambient noise includes explosions used for seismic exploration (up to 20,000 have been recorded off the coast of California in one year) and shipping traffic [9]. Natural ambient-noise is a broadband signal that exhibits a peak frequency close to 300 Hz, but can vary greatly due to weather conditions. Although natural noise is present in the 10–300 Hz band, its strength is not as significant as shipping noise in the same spectrum [9]. Ambient-noise has a center frequency close to 100 Hz, due to the relative strength of shipping noise.

Figure 4-6 [9] demonstrates the relative accuracy of Figure 4-5 and shows that the averages well represent noise strengths for ambient-noise spectra when viewed at single locations.

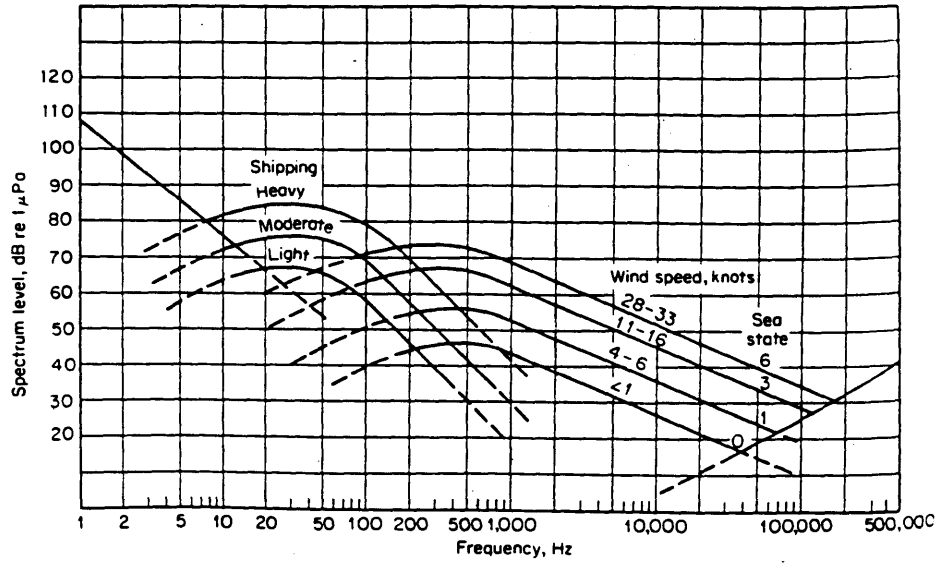


Figure 4-5: Average deep-water ambient-noise spectra

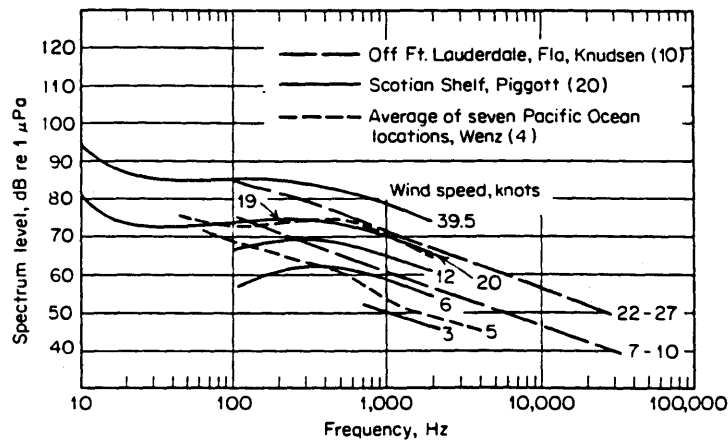


Figure 4-6: Noise spectra at coastal locations with wind speed as a parameter

## 4.2.2 Biologics

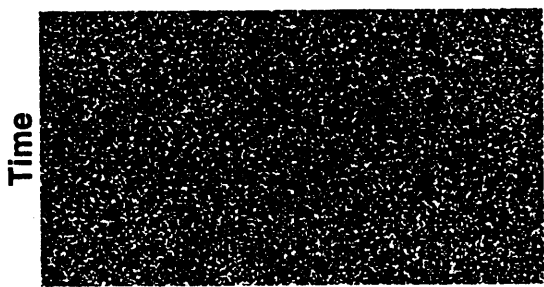
Biologics are living creatures in the ocean that create noise. Their signals vary in duration and frequency and the strength of their signals vary from place to place. Biologic noise-makers can be divided into three categories: certain shellfish (Crustacea), certain true fish, and marine mammals (Cetacea) [9]. Snapping shrimp are the primary noisemakers of the Crustacea. Their signals extend from 500 to 20 kHz, exhibiting a peak around 10 kHz. The largest contributor to noise in the true fish group are the croakers of Chesapeake Bay and other East Coast (US) locations. Croakers signals range from 100 to 10 kHz and have a peak frequency that varies from 500 Hz in late May and early June to 250 Hz in early July. Porpoises and dolphins dominate the mammal biologic noisemakers. The porpoise creates a 10 to 250 Hz frequency modulated whistle, while the dolphin is known for a wide variety of noises that are far too complex to analyze for the purpose of this thesis [9]. Overall, biologics tend to be a shorter duration signal than ambient noise, but can be just as troublesome, if not more, in the process of target detection.

## 4.2.3 Background Examples

Background environments range from rather benign, white-noise-like backgrounds to non-stationary, signal-like clutter (see following section). Figure 4-7 shows the gram and the amplitudes of the PSD for a white noise Gaussian time series. Figure 4-8 demonstrates the extreme opposite from white noise backgrounds, a gram abundant in narrowband, midband and broadband noise with random amplitude distributions.

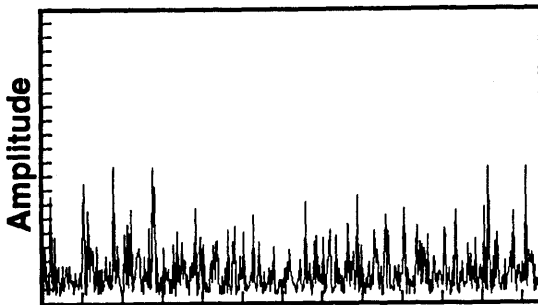
## 4.2.4 Clutter

Clutter is defined as a midband signal with randomly fluctuating amplitude and phase [8]. The random fluctuations imply that clutter is similar to noise when, in fact, it is signal-like because of the relatively narrow bandwidth of each feature. Signal-like clutter is the most troublesome of the unwanted background signals because it can often be mistaken for a piece of the signal because of its shape and size. However,



Frequency

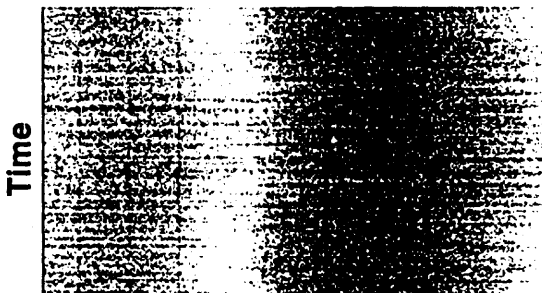
Gram



Frequency

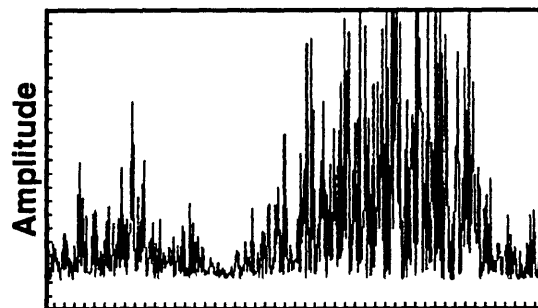
ASCAN

Figure 4-7: White Noise Gram and corresponding Amplitude Scan (ASCAN)



Frequency

Gram



Frequency

ASCAN

Figure 4-8: Non-Quiescent Gram and ASCAN

clutter mitigation is possible by examining the background only bands or *outbands* of the spectrum [7]. This thesis does not incorporate clutter modeling into simulations, but we do consider its theoretical implications later in the non-ideal energy band detector (Chapter 7). Clutter modeling has previously been analyzed and applied to the LRT in [7].

# Chapter 5

## Optimal Processing

Previously we have validated the statistical model for ocean acoustic data and explained our data processing pipeline, developed the theory behind optimal detection and outlined our background and signal models. This chapter will develop the Neyman-Pearson optimal LRT detector for the scenario previously outlined in this thesis.

### 5.1 Signal and Background Density Functions

First, we define two conceivable time-series inputs to the detector,

$$\begin{aligned}H_0 : x(t) &= b(t) \\ H_1 : x(t) &= s(t) + b(t),\end{aligned}$$

where  $s(t)$  is signal and  $b(t)$  is background noise. The first piece of the detector is the A/D converter (see Figure 2-1) which yields

$$\begin{aligned}H_0 : x_n &= b_n \\ H_1 : x_n &= s_n + b_n.\end{aligned}$$

Next the data is processed by a DFT and becomes

$$\begin{aligned} H_0 & : \underline{X}_{nj} = \underline{B}_{nj} \\ H_1 & : \underline{X}_{nj} = \underline{S}_{nj} + \underline{B}_{nj}, \end{aligned}$$

where  $\underline{X}(k)$  signifies the complex output of the DFT. The DFTs are computed on time epochs of length  $I$ . The individual scans are indexed by  $n$ , feature regions by  $m$  and frequency pickets are by  $k$ . The PSD is generated by magnitude-squaring the complex output, yielding two exponential PDF's (see Appendix A) with mean and standard deviation reprinted here from Chapter 4

$$E(z_{nk}^m | H_l) = \{\text{var}(z_{nk}^m | H_l)\}^{\frac{1}{2}} = \begin{cases} \mu_k^m, & l = 0 \\ \mu_k^m + \alpha\phi_m\lambda_k^m & l = 1 \end{cases} \quad (5.1)$$

Now we have all the parts necessary to write the inband PDFs for  $z_{nk}^m$  under each hypothesis  $\{H_l : l = 0, 1\}$ ,

$$p_{z_{nk}^m | H_l}(z_{nk}^m | H_l) = \frac{1}{E\{z_{nk}^m | H_l\}} \exp\left\{-\frac{z_{nk}^m}{E\{z_{nk}^m | H_l\}}\right\}. \quad (5.2)$$

The outband PDFs are identical under  $H_1$  and  $H_0$  by definition.

The joint probability density function of the vector  $\underline{z}$  is the product of the independent<sup>1</sup> exponential distributions, e.g.

$$p_{\underline{z} | H_l}(\underline{z} | H_l) = \prod_n \prod_m \prod_k p_{z_{nk}^m | H_l}(z_{nk}^m | H_l). \quad (5.3)$$

## 5.2 LRT Derivation

Since the outband PDFs are identical under hypothesis  $H_0$  and  $H_1$ , the LRT is only a function of the inband vector  $\underline{z}$ . Using Equation 3.1 with the joint PDF of

---

<sup>1</sup>It can be shown that the independent Gaussian input assumption of Chapter 2 leads to independent exponential distributions.



Equation 5.3,

$$L(\underline{z}) = \frac{\prod_n \prod_m \prod_k \frac{1}{E(z_{nk}^m | H_1)} \exp \left\{ -\frac{z_{nk}^m}{E(z_{nk}^m | H_1)} \right\}}{\prod_n \prod_m \prod_k \frac{1}{E(z_{nk}^m | H_0)} \exp \left\{ -\frac{z_{nk}^m}{E(z_{nk}^m | H_0)} \right\}} \underset{\hat{H}(y)=H_0}{\overset{\hat{H}(y)=H_1}{\geq}} \eta, \quad (5.4)$$

where

$$\underline{z}^T = [z_{00}^0 z_{01}^0 \cdots z_{N-1 K_m-1}^{M-1}]. \quad (5.5)$$

Note that the outband PDFs will simply cancel in Equation 5.4. To simplify this equation, let us take the natural log and in doing so define,

$$\ln\{L(\underline{z})\} = y, \quad (5.6)$$

and

$$\ln\{\eta\} = \gamma.$$

Now consider the result

$$y = \sum_{n=0}^{N-1} \sum_{m=0}^{M-1} \sum_{k=0}^{K_m-1} \left( -\ln \overline{\{z_{nk}^m | H_1\}} - \frac{z_{nk}^m}{E(z_{nk}^m | H_1)} + \ln \overline{\{z_{nk}^m | H_0\}} + \frac{z_{nk}^m}{E(z_{nk}^m | H_0)} \right) \underset{\hat{H}(y)=H_0}{\overset{\hat{H}(y)=H_1}{\geq}} \gamma, \quad (5.6)$$

where the overbar signifies the mean or expected value, i.e.

$$\bar{x} = E(x),$$

$$y = \sum_{n=0}^{N-1} \sum_{m=0}^{M-1} \sum_{k=0}^{K_m-1} \left( -\ln \frac{E(z_{nk}^m | H_1)}{E(z_{nk}^m | H_0)} + z_{nk}^m \frac{\overline{\{z_{nk}^m | H_1\}} - \overline{\{z_{nk}^m | H_0\}}}{E(z_{nk}^m | H_1) E(z_{nk}^m | H_0)} \right) \underset{\hat{H}(y)=H_0}{\overset{\hat{H}(y)=H_1}{\geq}} \gamma. \quad (5.7)$$

Notice that the first part of the sum in Equation 5.7 is simply a constant which can be incorporated into the threshold  $\gamma$ . Remove this constant and plug in the mean values from Equations 4.3 and 4.2 and we get

$$y = \sum_{n=0}^{N-1} \sum_{m=0}^{M-1} \sum_{k=0}^{K_m-1} z_{nk}^m \left( \frac{\mu_k^m + \alpha \phi_m \lambda_k^m - \mu_k^m}{\mu_k^m (\mu_k^m + \alpha \phi_m \lambda_k^m)} \right) \begin{array}{c} \hat{H}(y)=H_1 \\ \geq \\ < \\ \hat{H}(y)=H_0 \end{array} \gamma_2.$$

This becomes

$$y = \sum_{m=0}^{M-1} \sum_{k=0}^{K_m-1} \left( \frac{\alpha \phi_m \lambda_k^m}{\mu_k^m + \alpha \phi_m \lambda_k^m} \right) \frac{1}{\mu_k^m} \sum_{n=0}^{N-1} z_{nk}^m \begin{array}{c} \hat{H}(y)=H_1 \\ \geq \\ < \\ \hat{H}(y)=H_0 \end{array} \gamma_2.$$

Let us define

$$\tilde{s}_k^m \equiv \alpha \frac{\phi_m \lambda_k^m}{\mu_k^m} \quad (5.8)$$

to be the background normalized signal model. We can similarly treat

$$\tilde{z}_k^m \equiv \frac{\beta_k^m}{\mu_k^m} \quad (5.9)$$

as the background normalized ASCAN where the unnormalized ASCAN,  $\beta_k^m$ , is given by

$$\beta_k^m \equiv \frac{1}{N} \sum_{n=0}^{N-1} z_{nk}^m. \quad (5.10)$$

Note that under  $H_0$

$$E\{\tilde{z}_k^m\} = \frac{E\{\beta_k^m\}}{\mu_k^m} = \frac{E\{z_{nk}^m | H_0\}}{\mu_k^m} = 1, \text{ and}$$

$$\text{var}\{\tilde{z}_k^m\} = \frac{\text{var}\{\beta_k^m\}}{(\mu_k^m)^2} = \frac{\text{var}\{z_{nk}^m\}}{N(\mu_k^m)^2} = \frac{1}{N}.$$

Thus the normalized ASCAN is a consistent<sup>2</sup> estimate of the data ASCAN. A similar

---

<sup>2</sup>By *consistency* we mean the variance approaches zero as  $N$  approaches infinity.

analysis for the  $H_1$  case yields a consistent estimate with mean and variance proportional to the signal strength. The normalized notation we have developed provides rather simple data means under the hypothesis  $\{H_l : l = 0, 1\}$ ,

$$E(\tilde{z}_k^m | H_l) = \begin{cases} 1, & l = 0 \\ 1 + \tilde{s}_k^m & l = 1 \end{cases} \quad (5.11)$$

Now we can write Equation 5.8 as

$$y \equiv \sum_{m=0}^{M-1} \sum_{k=0}^{K_m-1} \frac{\tilde{s}_k^m}{1 + \tilde{s}_k^m} \tilde{z}_k^m \underset{\hat{H}(y)=H_0}{\overset{\hat{H}(y)=H_1}{\gtrless}} \gamma_3. \quad (5.12)$$

Consider the first and second moments of the detection metric  $y$

$$E(y | H_j) = \begin{cases} \sum_{m=0}^{M-1} \sum_{k=0}^{K_m-1} \frac{\tilde{s}_k^m}{1 + \tilde{s}_k^m} & j = 0 \\ \sum_{m=0}^{M-1} \sum_{k=0}^{K_m-1} \tilde{s}_k^m & j = 1 \end{cases}, \quad (5.13)$$

$$\text{var}(y | H_j) = \begin{cases} \frac{1}{N} \sum_{m=0}^{M-1} \sum_{k=0}^{K_m-1} \left( \frac{\tilde{s}_k^m}{1 + \tilde{s}_k^m} \right)^2 & j = 0 \\ \frac{1}{N} \sum_{m=0}^{M-1} \sum_{k=0}^{K_m-1} (\tilde{s}_k^m)^2 & j = 1 \end{cases} \quad (5.14)$$

Let us now normalize Equation 5.12 to zero mean and unity variance under the  $H_0$  case and define our normalized threshold as  $\sigma$ . The normalized detection metric  $\tilde{y}$  is now [2]

$$\tilde{y} = \sqrt{N} \frac{\sum_{m=0}^{M-1} \sum_{k=0}^{K_m-1} \left[ \frac{\tilde{s}_k^m}{1 + \tilde{s}_k^m} (\tilde{z}_k^m - 1) \right]}{\left[ \sum_{m=0}^{M-1} \sum_{k=0}^{K_m-1} \left( \frac{\tilde{s}_k^m}{1 + \tilde{s}_k^m} \right)^2 \right]^{1/2}} \underset{\hat{H}(y)=H_0}{\overset{\hat{H}(y)=H_1}{\gtrless}} \sigma. \quad (5.15)$$

# Chapter 6

## Performance Assessment

The signal-to-noise ratio (SNR) and deflection characteristic ( $d$ ) are useful tools by which performance can be predicted with relative degrees of accuracy. It is possible to measure SNR or  $d$  at any number of points in the detection process. This chapter examines several such computations and attempts to exploit their relationships in order to gain insight into detector performance.

The ratio of energies SNR computation (referred to as SNR in section 3.4) and deflection characteristic assume stationary processes in the time period for which we are computing the metrics. If the process is non-stationary, the metrics are changing over the period which we are integrating. For non-stationary processes it is more meaningful to compute the metrics for smaller chunks of the process that are relatively stationary.

One of the difficulties of SNR or  $d$  measurement is the separation of signal from noise in order to construct a meaningful ratio. Regardless, this chapter develops useful metrics for separable signals and noise, and consequently lends insight into non-separable real-data detection scenarios.

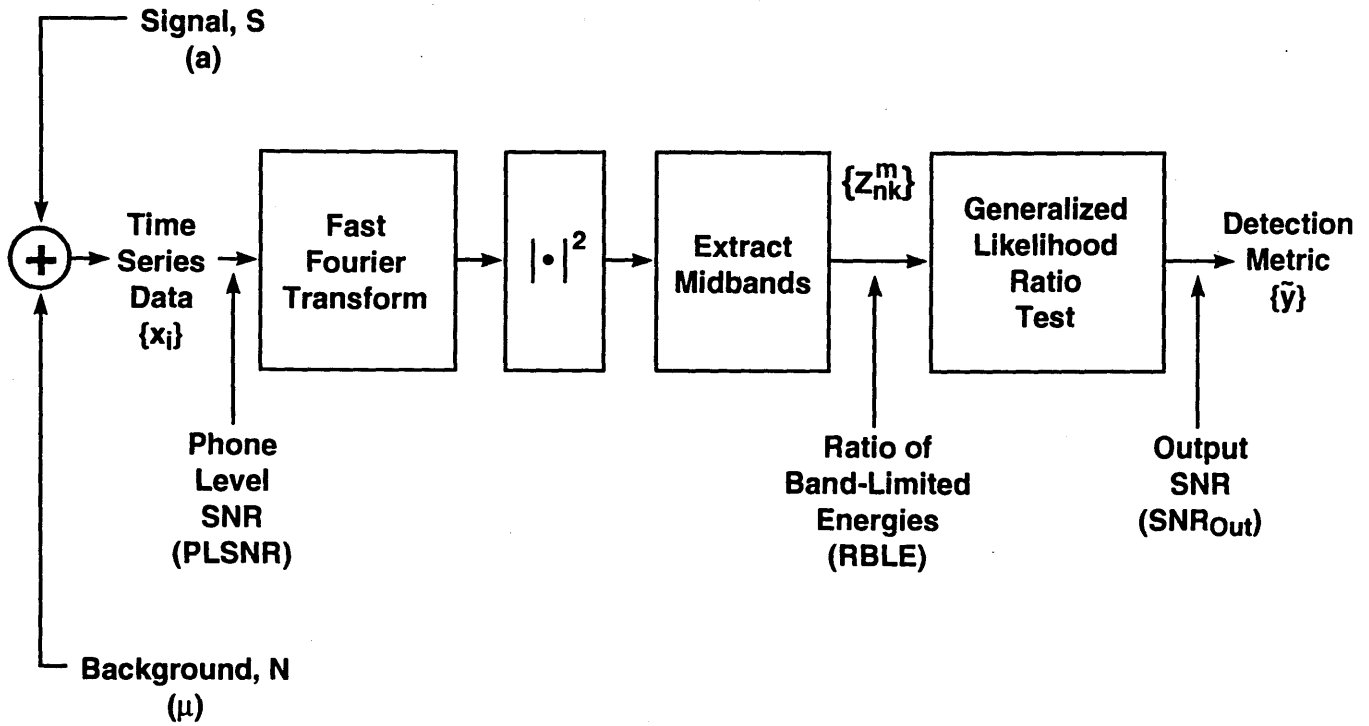


Figure 6-1: PLSNR, RBLE & SNRO

## 6.1 Performance Metrics Throughout the Detection Process

Figure 6-1 is a simplified diagram of the discrete portion of the detection process. We will measure SNR at three distinct points in the process: the phone level, the bandlimited phone level and the output. Each SNR measurement occurs further down the processing chain than the last and so should be a better prediction of detector performance.

### 6.1.1 Phone Level Signal-to-Noise Ratio

The phone level SNR (PLSNR) is measured at the output of the analog-to-digital converter. Using the notation of Chapter 2, we will adopt  $s$  and  $b$  for the separable

signal and noise components of our data. Thus, we define

$$\begin{aligned}
E(x_i|H_0) &= b_i, \\
E(x_i|H_1) &= b_i + s_i, \\
E(x_{nj}|H_0) &= B_{nj}, \\
E(x_{nj}|H_1) &= B_{nj} + S_{nj},
\end{aligned}$$

and we can write

$$\text{PLSNR} \equiv \frac{\text{Average Signal Power}}{\text{Average Noise Power}} = \frac{\sum_{i=0}^{I-1} s_i^2}{\sum_{i=0}^{I-1} b_i^2} = \frac{\sum_{j=0}^{I-1} |S_{nj}|^2}{\sum_{j=0}^{I-1} |B_{nj}|^2}, \quad (6.1)$$

where the final equality arises from Parseval's Theorem.

### 6.1.2 Ratio of Bandlimited Energies

The ratio of bandlimited energies (RBLE) is similar to PLSNR, except now we are bandlimiting to bands of interest only, specifically inbands. PLSNR can be viewed as a broadband SNR measurement. However, extracting the midband features of our data is essentially a filtering operation which establishes a receiver bandwidth for the detector corresponding to the inbands. This filtering operation increases the SNR (i.e.  $\text{RBLE} \geq \text{PLSNR}$ ) because we still have the same<sup>1</sup> energy in the signal bands of interest, but we are reducing the noise bandwidth. The result is a ratio of inbands,

$$\text{RBLE} \equiv \frac{\text{Average Inband Signal Power}}{\text{Average Inband Noise Power}} = \frac{\sum_{m=0}^{M-1} \sum_{k=0}^{K_m-1} \alpha \phi_m \lambda_k^m}{\sum_{m=0}^{M-1} \sum_{k=0}^{K_m-1} \mu_k^m} = \frac{\alpha}{\sum_{m=0}^{M-1} \sum_{k=0}^{K_m-1} \mu_k^m}. \quad (6.2)$$

### 6.1.3 Output Signal-to-Noise Ratio

When the deflection characteristic is measured at the output of the LRT processor, we obtain the Output SNR metric or the SNRO. We can construct the SNRO using

---

<sup>1</sup>It is important to note that we are also losing some broadband signal energy, however, as the results will show, the overall effect is an increase in the SNR.

the deflection characteristic SNR definition (Equation 3.5) and the LRT y-metric moments (Equations 5.13 and 5.14)

$$\begin{aligned} [E(y | H_1) - E(y | H_0)]^2 &= \left[ \sum_{m=0}^{M-1} \sum_{k=0}^{K_m-1} \tilde{s}_k^m - \sum_{m=0}^{M-1} \sum_{k=0}^{K_m-1} \frac{\tilde{s}_k^m}{1+\tilde{s}_k^m} \right]^2 \\ &= \left[ \sum_{m=0}^{M-1} \sum_{k=0}^{K_m-1} \frac{(\tilde{s}_k^m)^2}{1+\tilde{s}_k^m} \right]^2 \end{aligned}$$

and dividing by the variance under  $H_0$ ,

$$\text{SNRO} = N \frac{\left[ \sum_{m=0}^{M-1} \sum_{k=0}^{K_m-1} \frac{(\tilde{s}_k^m)^2}{1+\tilde{s}_k^m} \right]^2}{\sum_{m=0}^{M-1} \sum_{k=0}^{K_m-1} \left( \frac{\tilde{s}_k^m}{1+\tilde{s}_k^m} \right)^2}. \quad (6.3)$$

Comparing the SNRO to the LRT (Equation 5.12) we see that the SNRO is simply the square of the expected value of the LRT ( $E\{z_{nk}^m\} = s_k^m$ ) for the  $H_1$  case. Thus, in essence the LRT is estimating, based on the assumed model and available data, the SNRO, and indicating a target present if the estimate is large enough. The output SNR utilizes all of the model information used by the LRT and so the mean LRT reduces to the SNRO under the target present hypothesis. The major difference between the RBLE and PLSNR measurements and the SNRO is that the output SNR measures the difference in hypothesis means as compared to the standard deviation, rather than a simple ratio of filtered (RBLE) or unfiltered (PLSNR) signal-to-noise ratios.

## 6.2 A Simple Example

Figure 4-4 is a simple model we will use as an example to compute the PLSNR, RBLE and SNRO. Note that one could also compute the SNRs for a complex model such as Figure 4-3 using the same method, just changing the values of constants  $a, K, M$  and the vectors  $\lambda, \phi$  and  $\mu$  to match the more complex model.

Using the model of Figure 4-4 and assuming both  $s_k^m = 1 + a$  and  $\mu_k^m = 1$  are

constant for all  $m$  and  $k$ , the equations simplify to:

$$\text{PLSNR} = \left(\frac{MK}{I/2}\right)\left(\frac{a}{\mu}\right), \quad (6.4)$$

$$\text{RBLE} = \left(\frac{a}{\mu}\right), \text{ and} \quad (6.5)$$

$$\text{SNRO} = NMK \left(\frac{a}{\mu}\right)^2. \quad (6.6)$$

Notice that the three SNRs are all functions of the fractional signal bandwidth  $\frac{MK}{I/2}$ , the single-bin SNR,  $\frac{a}{\mu}$ , and the time-frequency bandwidth  $NMK$ . The time-frequency bandwidth is a simple function involving our sampling rate and scan parameters. If we sample at a rate  $T_s$ , we define the *dwelt time* as  $T = IT_s$ , whose inverse,  $\frac{1}{IT_s}$ , is frequency resolution. The time-frequency bandwidth can be defined in these terms as the product of dwelt time and receiver bandwidth,

$$\text{BT} = (NIT_s)\left(\frac{MK}{IT_s}\right) = NMK. \quad (6.7)$$

Using the above equations it is easy to rewrite any of them in terms of one another, here is how they relate:

$$\text{RBLE} = \frac{I}{2MK} (\text{PLSNR}) \quad (6.8)$$

$$\text{SNRO} = NMK (\text{RBLE})^2. \quad (6.9)$$

There are several relationships of note among the three SNR computations shown here. First, RBLE reduces to PLSNR when the signal bandwidth covers the entire spectrum (i.e.  $MK = I/2$ .) Secondly, increasing  $M, K, N$  and  $a$  and decreasing  $\mu$  improves all of the SNRs. Third, RBLE has a gain over PLSNR proportional to the fractional bandwidth occupied by the inbands. Finally, the gain associated with SNRO is proportional to the time-frequency bandwidth.



## 6.3 Performance Bounds

Now that we have developed the LRT and several useful SNR measurements, it is relatively straight-forward to construct bounds and approximations which demonstrate the limits of performance of the optimal LRT detector. Consider the optimal performance bound which can be found by analyzing the respective distributions of the output statistic,  $y$ , for the  $H_0$  and  $H_1$  cases. We can then compare them so that we can construct a receiver operating characteristic (ROC) or  $P_D$  versus  $P_F$  curve, which can be a cumbersome process. There are, however, methods which can compute ROC bound approximations using deterministic information about the data.

### 6.3.1 Chernoff Bound Approximation

The performance of the LRT can be approximated by the following modified Chernoff bound [10],

$$P_F \approx \frac{\exp[\mu(s_m) - s_m \dot{\mu}(s_m)]}{\sqrt{2\pi s_m^2 \ddot{\mu}(s_m)}}, \quad (6.10)$$

$$P_D \approx 1 - \frac{\exp[\mu(s_m) + (1 - s_m) \dot{\mu}(s_m)]}{\sqrt{2\pi(1 - s_m)^2 \ddot{\mu}(s_m)}}, \quad (6.11)$$

where  $P_F$  and  $P_D$  are the false-alarm and detection probabilities respectively. For  $0 \leq s \leq 1$ ,  $\mu(s)$  is defined as [10]

$$\mu(s) \equiv \ln \left\{ \int d\vec{\mathbf{Z}} [p_{Z|H_1}(\mathbf{Z}|H_1)]^s [p_{Z|H_0}(\mathbf{Z}|H_0)]^{1-s} \right\}, \quad (6.12)$$

where  $\mathbf{Z}$  is a random vector of data under the familiar hypotheses  $H_1$  and  $H_0$ . For the bounds we define

$$\dot{\mu}(s) \equiv \frac{d\mu}{ds} \text{ and } \ddot{\mu}(s) \equiv \frac{d^2\mu}{ds^2} \quad (6.13)$$

as the first and second derivatives of  $\mu(s)$ . These modified Chernoff bound approximations assume that [6]

$$s_m \sqrt{2\pi \dot{\mu}(s_m)} > 3 \text{ and } (1 - s_m) \sqrt{2\pi \ddot{\mu}(s_m)} > 3. \quad (6.14)$$

Using our previously defined signal,  $s_k^m$ , and background,  $\mu_k^m$  and [6], we can show that

$$\mu(s) = \sum_m \sum_k \{(1-s) \ln(s_k^m + \mu_k^m) + s \ln(\mu_k^m) - \ln[(1-s)s_k^m + \mu_k^m]\},$$

$$\dot{\mu}(s) = \sum_m \sum_k \left[ \frac{s_k^m}{(1-s)s_k^m + \mu_k^m} - \ln\left(\frac{s_k^m + \mu_k^m}{\mu_k^m}\right) \right] \text{ and,}$$

$$\ddot{\mu}(s) = \sum_m \sum_k \left( \frac{s_k^m}{(1-s)s_k^m + \mu_k^m} \right)^2.$$

Now if we vary the parameter  $s$  it is possible to trace out an approximation to the ROC curve.

### 6.3.2 Error Function Approximation

Another useful approximation on  $P_D$  and  $P_F$  for the LRT is achieved by using the Q or error function. The error function simply integrates over a given portion of a Gaussian density function,

$$\text{ERFC}(x) = \frac{1}{\sqrt{2\pi}} \int_{-\infty}^x e^{-t^2/2}. \quad (6.15)$$

If we assume, using the Central Limit Theorem, that the detection metric ( $y$ ) takes on a Gaussian distribution when we integrate over a large enough time-frequency bandwidth, we can propose the following approximation on performance,

$$P_F = \text{ERFC}(-\gamma), \quad (6.16)$$

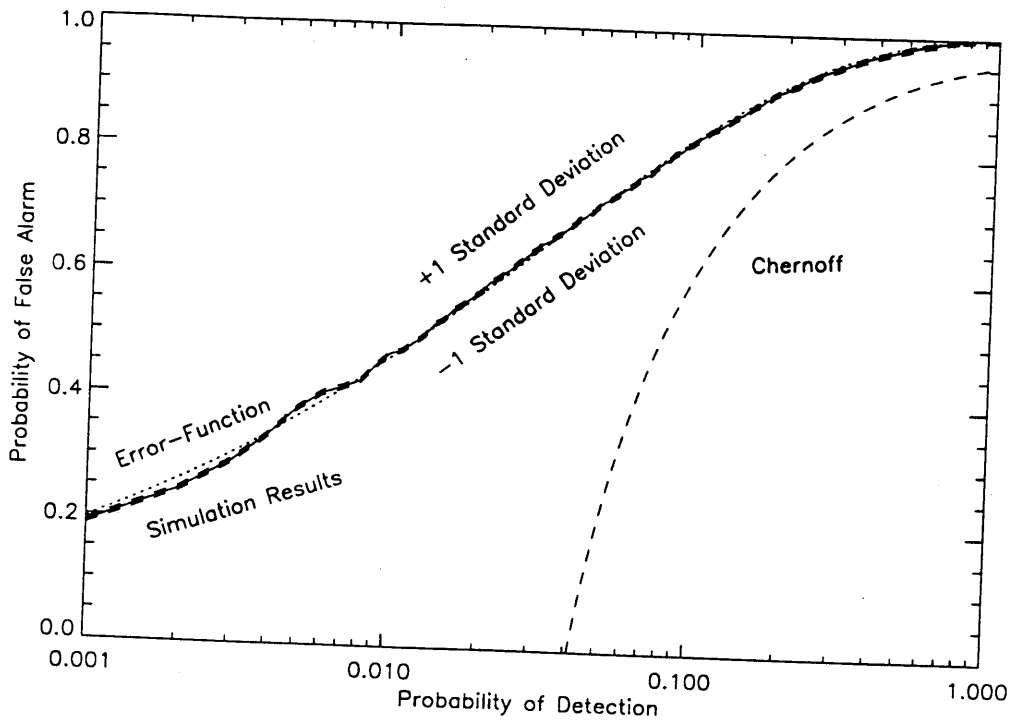


Figure 6-2: Error Function, Simulation and Chernoff Boundries

$$P_D = \text{ERFC}(E(\tilde{y}|H_1) - \gamma) = \text{ERFC}(\sqrt{\text{SNRO}} - \gamma). \quad (6.17)$$

Note that  $\gamma$  is the threshold we set and  $\sqrt{\text{SNRO}}$  is the difference in hypothesis means or the distance between the mean values of the two Gaussian distributions. Note that the SNRO also normalizes the variance to one and the mean to zero so that we need to make no adjustments when applying the error function.

### 6.3.3 Simulation Analysis

It is relatively simple to construct a simulation, utilizing the assumed measurement statistics, to verify the accuracy of these approximations. Figure 6-4 shows the three bounds for a simulation using a time frequency bandwidth of 2000 bins and a single-bin SNR of 0.05. Note how similar the error function bound is to the LRT simulation bound. The Chernoff approximation is much more pessimistic than the true boundary for this particular example.

# Chapter 7

## LRT and EBD Analysis

Now that we have laid out the LRT algorithm used to process data and optimize performance, we will, in this section, demonstrate the optimality of the LRT in closed form. Our demonstration consists of comparing to an Energy Band Detector (EBD). We will consider both ideal and non-ideal EBDs and look at the performance of the LRT and EBDs as we vary the number of signal bands in our signal model.

In our analysis, we will use the deflection characteristic (d) to compare our various detection algorithms. We can justify using this as a performance metric if we consider the results of the simulation in Section 6.4.3. There we determined that the error function performance boundaries were very close to the simulation performance bounds. Recall also that the error function approximations depend only on a fixed threshold  $\gamma$  and the deflection characteristic.

### 7.1 Number of Feature Regions Utilized

Let us assume we have  $M$  feature regions each of length  $K$  bins,  $N$  time epochs, signal power  $a$  and a uniform background power of magnitude one (see Figure 4-4). The ideal energy band detector (EBD) sums the energy in each bin  $k$  over all  $m$  feature regions and  $n$  time epochs,

$$y = \sum_n \sum_m \sum_k z_{nk}^m, \quad (7.1)$$

where  $z_{nk}^m$  is the power spectral density of the signal and background noise waveforms. Recall also that the deflection metric is,

$$d = \frac{|E(y|H_1) - E(y|H_0)|^2}{\text{var}(y|H_0)}. \quad (7.2)$$

Note that we will analyze flat band weighting in this section, which produces identical deflection characteristics for both the EBD and the LRT.

We can solve for the expected values under both the signal present and the noise only hypothesis,

$$\begin{aligned} E\{y|H_0\} &= E\left\{\sum_n \sum_m \sum_k z_{nk}^m | H_0\right\} \\ &= \sum_n \sum_m \sum_k E\{z_{nk}^m | H_0\} \\ &= \sum_n \sum_m \sum_k (1) = NMK \end{aligned}$$

$$\begin{aligned} E\{y|H_1\} &= E\left\{\sum_n \sum_m \sum_k z_{nk}^m | H_1\right\} \\ &= \sum_n \sum_m \sum_k E\{z_{nk}^m | H_1\} \\ &= \sum_n \sum_m \sum_k (1 + a) = NMK(1 + a). \end{aligned}$$

A similar analysis yields,

$$\text{var}\{y|H_0\} = NMK.$$

Then we can plug these equations into our deflection metric to compute,

$$d_{\text{EBD}}(M|M) = a^2 NMK, \quad (7.3)$$

where the notation  $d_{\text{EBD}}(q|r)$  indicates that this is the deflection when summing  $q$

features given  $r$  features are true.

Note that if we sum over  $L$  of  $M$  possible feature regions and  $L < M$ , we suffer a performance reduction of  $\frac{L}{M}$  from the optimum EBD which would include all  $M$  features.

$$d_{\text{EBD}}(L|L < M) = a^2NK \frac{L}{M}. \quad (7.4)$$

Consider, if you will, the effect of summing over  $L$  feature regions when in fact there are only  $M$  regions with signal, where  $M < L$ . The  $H_0$  analysis will not change, however the expected value of  $H_1$  will,

$$E\{y|H_1\} = NLK(1) + NMK(a).$$

Now the deflection metric becomes,

$$d_{\text{EBD}}(L|L > M) = a^2NK \frac{M^2}{L}, \quad (7.5)$$

which also reduces to the allbands case when  $L = M$ . This satisfyingly tells us that were we to choose  $x + 1$  feature regions when  $x$  existed, we would suffer the same performance degradation as choosing  $x$  feature regions when  $x + 1$  are present. However, consider a case where we do not know how many feature regions will be present in a real signal, but we are aware of the locations of the possible feature regions. We can guess an average number of feature regions to include out of the total, but are we better off erring on the side of choosing too many feature regions, or choosing too few? The answer is, not surprisingly, choosing too many. Increased processing bandwidth more often helps performance than hinders it. We can prove this solution by considering a case where we fix the number of feature regions to be processed ( $L$ ) and vary the number of regions present in the signal from  $M = L + J$  to  $M = L - J$ , for  $J \geq 0$ . If  $M = L + J$  then  $M > L$  and the deflection metric differs by a factor of  $\frac{M-J}{M}$ . However, if  $M = L - J$  then  $L > M$  and the deflection metric is degraded to a factor of  $\frac{M}{M+J}$ . Let us examine now the ratio of performance degradation between the  $M > L$  case and the  $L > M$  case,

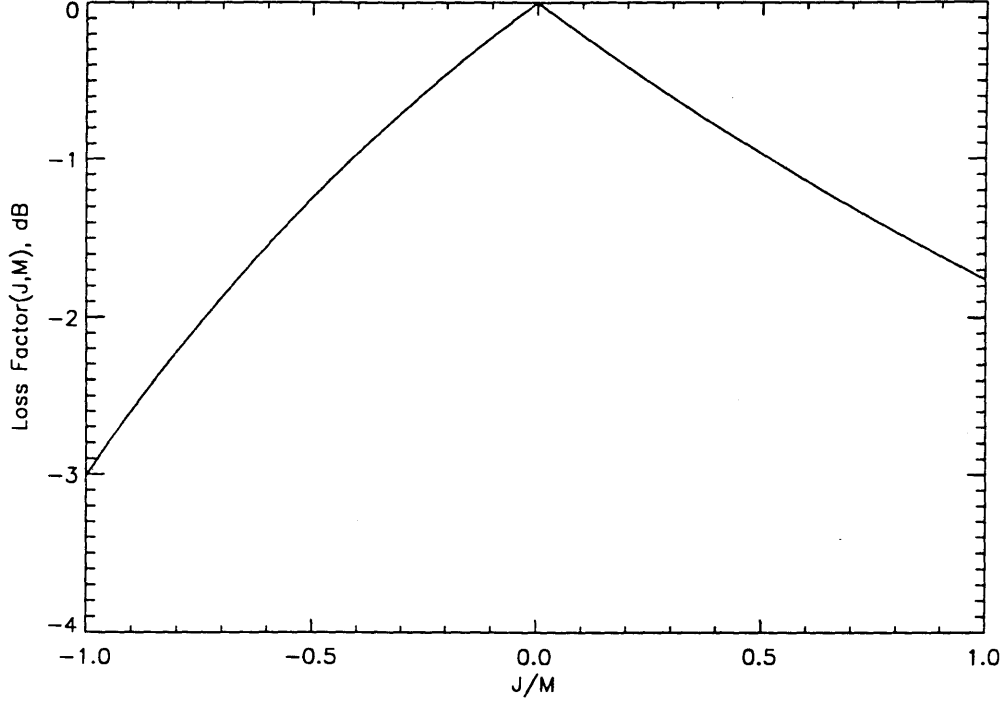


Figure 7-1:  $J/M$  Versus Loss Factor  $\epsilon(J, M)$  for EBD

$$\frac{(M - J)/M}{M/(M + J)} = \frac{(M - J)(M + J)}{M^2} \leq 1. \quad (7.6)$$

Notice that when  $J = 0$  the two cases will reduce to the  $L = M$  case, but for all  $J > 0$ , the ratio between scaling factors for performance is always less than one, implying that we are better off with  $L > M$ .

We define a loss factor of  $\epsilon(J, M)$  so that,

$$\epsilon(J, M) = 10 \log \left( \frac{d_{\text{EBD}}(L = J + M | M)}{d_{\text{EBD}}(L = M | M)} \right) = \begin{cases} \frac{1}{1 + J/M} & J > 0 \\ 1 + J/M & J \leq 0 \end{cases}, \quad (7.7)$$

and plot  $\epsilon(J, M)$  versus  $J/M$  in Figure 7.1.

Figure 7.1 tells us that if we can not choose the exact number of feature regions, we can tolerate greater error in the number by choosing a number of feature regions more likely to be greater than the actual number of feature regions.

## 7.2 LRT versus EBD

Recall the previously defined LRT,

$$y \equiv \sum_{m=0}^{M-1} \sum_{k=0}^{K_m-1} \frac{\tilde{s}_k^m}{1 + \tilde{s}_k^m} z_k^m \underset{\hat{H}(y)=H_0}{\overset{\hat{H}(y)=H_1}{\gtrless}} \gamma, \quad (7.8)$$

where  $\tilde{s}_k^m$  is the signal model. In Chapter 6, the LRT SNRO was defined as:

$$\text{SNRO} = N \frac{\left[ \sum_{m=0}^{M-1} \sum_{k=0}^{K_m-1} \frac{(\tilde{s}_k^m)^2}{1 + \tilde{s}_k^m} \right]^2}{\sum_{m=0}^{M-1} \sum_{k=0}^{K_m-1} \left( \frac{\tilde{s}_k^m}{1 + \tilde{s}_k^m} \right)^2}. \quad (7.9)$$

If we choose  $\tilde{s}_k^m = a$  note that the deflection metric reduces to the equally weighted bands of the energy band detector,  $a^2 N M K$ .

Let us examine a simple case where we weight the bands differently and see what the benefit is of the LRT. Let us choose  $M$  bands of signal and background that are weighted such that  $\tilde{s}_k^m = a_m$ . Background is still flat and equal to one. The  $E\{y|H_0\}$  and the  $\text{var}\{y|H_0\}$  stay the same since background still equals one. However, looking at  $H_1$ ,

$$\begin{aligned} E\{y|H_1\} &= E\left(\sum_n \sum_m \sum_k z_{nk}^m\right) \\ &= \sum_n \sum_k E\left(\sum_m z_{nk}^m\right) \\ &= NK \sum_m (1 + a_m) \end{aligned}$$

This means the EBD deflection metric in the weighted bands case looks like,

$$d = \frac{NK}{M} \left(\sum_m a_m\right)^2 \quad (7.10)$$

Note that when  $a_m = a \forall m$ ,  $d$  reduces to  $a^2 N M K$  which is identical to the



flatband deflection characteristic.

If we consider the same feature regions as above for the LRT, the deflection metric is defined as,

$$\text{SNRO} = N \frac{\left[ \sum_m \sum_k \frac{(\tilde{s}_k^m)^2}{1+\tilde{s}_k^m} \right]^2}{\sum_m \sum_k \left( \frac{\tilde{s}_k^m}{1+\tilde{s}_k^m} \right)^2} = NK \frac{\left[ \sum_m \frac{(a_m)^2}{1+a_m} \right]^2}{\sum_m \left( \frac{a_m}{1+a_m} \right)^2}. \quad (7.11)$$

Let us define variables  $x$  and  $y$  such that

$$\begin{aligned} x &= a_m \\ y &= \frac{a_m}{1+a_m}. \end{aligned}$$

We can compute the sample cross-covariance of  $x$  and  $y$

$$\begin{aligned} \text{cov}(x, y) &= \overline{(x - \bar{x})(y - \bar{y})} \\ &= \frac{1}{M} \sum_m (a_m - \frac{1}{M} \sum_m a_m) \left( \frac{a_m}{1+a_m} - \frac{1}{M} \sum_m \frac{a_m}{1+a_m} \right) \\ &= \frac{1}{M} \sum_m \left[ \frac{a_m^2}{1+a_m} - \frac{1}{M} \left( \frac{a_m}{1+a_m} \right) \sum_m a_m - \frac{1}{M} a_m \sum_m \left( \frac{a_m}{1+a_m} \right) + \frac{1}{M^2} \sum_m a_m \sum_m \left( \frac{a_m}{1+a_m} \right) \right] \\ &= \frac{1}{M} \sum_m \left( \frac{a_m^2}{1+a_m} \right) - \frac{1}{M^2} \sum_m \left( \frac{a_m}{1+a_m} \right) \sum_m a_m - \frac{1}{M^2} \sum_m a_m \sum_m \left( \frac{a_m}{1+a_m} \right) + \frac{1}{M^2} \sum_m a_m \sum_m \left( \frac{a_m}{1+a_m} \right) \\ &= \frac{1}{M} \sum_m \left( \frac{a_m^2}{1+a_m} \right) - \frac{1}{M^2} \sum_m a_m \sum_m \left( \frac{a_m}{1+a_m} \right). \end{aligned}$$

Note that the sample cross-covariance is greater than or equal to zero under these circumstances, thus

$$\frac{1}{M} \sum_m \left( \frac{a_m^2}{1+a_m} \right) \geq \frac{1}{M^2} \sum_m a_m \sum_m \left( \frac{a_m}{1+a_m} \right)$$

which implies

$$\begin{aligned} \left[ \sum_m \left( \frac{a_m^2}{1+a_m} \right) \right]^2 &\geq \left[ \frac{1}{M} \sum_m a_m \sum_m \left( \frac{a_m}{1+a_m} \right) \right]^2 \\ \left[ \frac{\sum_m \left( \frac{a_m^2}{1+a_m} \right)}{\sum_m \left( \frac{a_m}{1+a_m} \right)} \right]^2 &\geq \left[ \frac{1}{M} \sum_m a_m \right]^2. \end{aligned}$$

If the above relationship is true, it must follow that

$$\frac{\left(\sum_m \left(\frac{a_m^2}{1+a_m}\right)\right)^2}{\sum_m \left(\frac{a_m}{1+a_m}\right)^2} \geq \frac{1}{M} \left(\sum_m a_m\right)^2 \quad (7.12)$$

because

$$\left[\sum_m \left(\frac{a_m}{1+a_m}\right)\right]^2 \leq M \sum_m \left(\frac{a_m}{1+a_m}\right)^2$$

due to the constraint that the sample variance of our variable  $y \geq 0$ .

Equation 7.12 tells us that the likelihood-ratio test deflection characteristic is always at least as good as the energy band detector. The two metrics are equivalent when all bands are weighted equally.

### 7.3 The Non-Ideal EBD and Signal-Like Clutter

The non-ideal EBD is a detector aimed at combatting the problem of signal-confusable clutter. It takes an estimate of noise clutter from the signal bins outside the signal feature regions and subtracts out the clutter-related noise estimate from the signal feature regions. The non-ideal EBD is written as,

$$y = \frac{1}{NM_i K} \sum_n \sum_{m_i} \sum_k z_{nk}^{m_i} - \frac{1}{NM_o K} \sum_n \sum_{m_o} \sum_k z_{nk}^{m_o} \quad (7.13)$$

where  $M_i$  is the number of signal feature regions with  $K$  bins and  $M_o$  is the number of feature regions with  $K$  bins lying outside the signal bins.

We can compute the squared deflection metric for the ideal and non-ideal EBDs in a noise-cluttered background environment. Let us define a probability that clutter noise will occur in a given bin as  $P_c$  and this clutter has a bin-level SNR of  $c$ . Recall that the bin-level SNR of the signal is  $a$ . Thus we have,

$$\Pr\{E(z_{nk}^m) = (1+c)|H_0\} = P_c$$

$$\begin{aligned}
\Pr\{E(z_{nk}^m) = 1|H_0\} &= 1 - P_C \\
\Pr\{E(z_{nk}^m) = (1 + a + c)|H_1\} &= P_C \\
\Pr\{E(z_{nk}^m) = (1 + a)|H_1\} &= 1 - P_C.
\end{aligned}$$

First let us consider the deflection characteristic of the non-ideal EBD,

$$\begin{aligned}
E\{y|H_0\} &= \left(\frac{NM_iK}{NM_iK}\right) [(1 + c)P_C + (1)(1 - P_C)] \\
&\quad - \left(\frac{NM_oK}{NM_oK}\right) [(1 + c)P_C + (1)(1 - P_C)] = 0,
\end{aligned}$$

$$\begin{aligned}
E\{y|H_1\} &= \left(\frac{NM_iK}{NM_iK}\right) [(1 + a + c)P_C + (1 + a)(1 - P_C)] \\
&\quad - \left(\frac{NM_oK}{NM_oK}\right) [(1 + c)P_C + (1)(1 - P_C)] \\
&= (cP_C + 1 + a) - (cP_C + 1) = a,
\end{aligned}$$

In order to compute the variance, let us start by calculating  $\text{var}(z_{nk}^m|H_0)$ ,

$$\begin{aligned}
\text{var}\{z_{nk}^m|H_0\} &= E[(z_{nk}^m)^2|H_0] - [E(z_{nk}^m|H_0)]^2 \\
&= P_C E[(z_{nk}^m)^2|H_0, c] + (1 - P_C) E[(z_{nk}^m)^2|H_0, 0] - [E(z_{nk}^m|H_0)]^2 \\
&= P_C [\sigma_{z_{nk}^m|H_0, c}^2 + E(z_{nk}^m|H_0, c)^2] + (1 - P_C) [\sigma_{z_{nk}^m|H_0, 0}^2 + E(z_{nk}^m|H_0, 0)^2] - [E(z_{nk}^m|H_0)]^2 \\
&= 2P_C(1 + c)^2 + 2(1 - P_C)(1)^2 - (1 + cP_C)^2 \\
&= 1 + 2cP_C + c^2P_C(2 - P_C),
\end{aligned}$$

where  $H_0, c$  denotes the null hypothesis with clutter and  $H_0, 0$  denotes the null hypothesis with no clutter. Thus the variance for the non-ideal EBD is

$$\begin{aligned}
\text{var}\{y|H_0\} &= \left(\frac{1}{NM_iK}\right)^2 NM_iK [1 + 2cP_C + c^2P_C(2 - P_C)] \\
&\quad - \left(\frac{1}{NM_oK}\right)^2 NM_oK [1 + 2cP_C + c^2P_C(2 - P_C)] \\
&= \frac{1 + 2cP_C + c^2P_C(2 - P_C)}{NK} \left(\frac{M_o + M_i}{M_o M_i}\right).
\end{aligned}$$

We can similarly compute the squared deflection characteristic for the ideal EBD,

$$E\{y|H_0\} = NM_iK[(1+c)P_C + (1)(1-P_C)] = NM_iK(1+cP_C),$$

$$E\{y|H_1\} = NM_iK[(1+a+c)P_C + (1+a)(1-P_C)] = NM_iK(cP_C + 1+a),$$

$$\text{var}\{y|H_0\} = NM_iK(1 + 2cP_C + c^2P_C(2 - P_C)).$$

If we compare the squared deflection metric of the non-ideal EBD to that of the ideal EBD we find,

$$\text{EBD}_{\text{non-ideal}} < \text{EBD}_{\text{ideal}}$$

$$\left( \frac{NM_iKa^2}{1 + 2cP_C + c^2P_C(2 - P_C)} \right) \left( \frac{M_o}{M_i + M_o} \right) < \left( \frac{NM_iKa^2}{1 + 2cP_C + c^2P_C(2 - P_C)} \right). \quad (7.14)$$

Looking only at the deflection characteristic it appears as if our non-ideal EBD is a wasted effort, since the fractional difference  $\frac{M_o}{M_i + M_o} < 1$ . However, in this case the deflection characteristic is misleading. The variance in both cases worsens with increasing  $c$ , and reduces to the non-clutter case when  $c = 0$ . The difference in hypothesis means for both the ideal and the non-ideal EBD is  $a$ , however, the hypothesis means for the non-ideal case remain fixed for all  $c$  while the means for the ideal EBD vary with  $c$ . For example, consider  $y_i$  and  $y_{ni}$ , the detection metrics for the ideal and non-ideal energy band detectors respectively,

$$E\{y_{ni}|H_1\} - E\{y_{ni}|H_0\} = E\{y_i|H_1\} - E\{y_i|H_0\} = a$$

$$E\{y_{ni}|H_0\} = 0 \forall c, \text{ however, } E\{y_i|H_0\} = NM_iK(1 + cP_C).$$

Consider the effect this varying mean will have on the false-alarm rate in Figure 7.3.

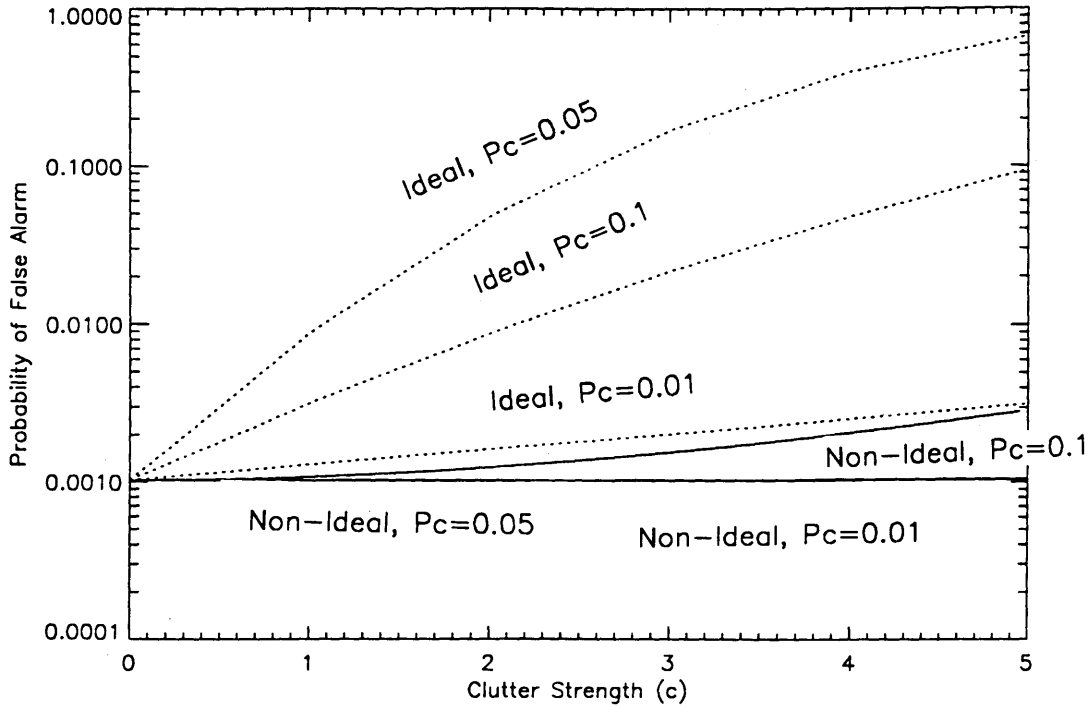


Figure 7-2:  $c$  versus  $P_F$  for various values of  $P_c$

As clutter strength increases,  $P_F$  grows for both the ideal and the non-ideal EBD. However,  $P_F$  increases much more rapidly due to the fixed threshold value. It is true that  $P_D$  changes as well, however its change is negligible compared to the large differences in  $P_F$ .

Note that the above relations correspond to a fixed threshold value of  $\gamma$ . If we could vary the threshold value with  $c$  we could achieve the performance of the EBD in the non-clutter scenario, however, we have no way of knowing a priori the value of  $c$  or  $P_c$ . Thus for noise-like clutter we can only estimate the clutter strength using a detector like the non-ideal EBD, and suffer the related degradation in detector performance in order to keep a relatively constant FAR.

# Chapter 8

## Background Estimators

So far we have only considered the known-background and known-signal cases. In real life, we do not know either the signal or the background and must construct parameter estimates to perform target detection. Recall the generalized likelihood ratio test (GLRT) mentioned in Chapter 3. The GLRT utilizes a library of presumed signal models. These estimates are stored for quick comparison to measured spectrograms. The GLRT also requires a background estimate, which is computed on the scene by a given algorithm designed to remove the signal-like components from a processed spectrogram. The better this algorithm, the more accurate the background estimate and, presumably, the better detection performance. Here we will consider one popular and widely used background estimation algorithm, the noise-spectral equalizer (NSE), and present a series of tests and guidelines intended to optimize its performance.

### 8.1 NSE

Noise spectrum equalizers, or NSE as it has become known, includes many slightly varied algorithms all with the same fundamental components, clipping and smoothing. The spectrum clipping consists of comparing  $z_i$  to an average  $\bar{z}_i$  of surrounding bins (see Figure 8-1),

$$\bar{z}_i = \frac{1}{S-G} \sum_{j=i-S/2}^{i-G/2} z_j + \sum_{j=i+G/2}^{i+S/2} z_j \quad (8.1)$$

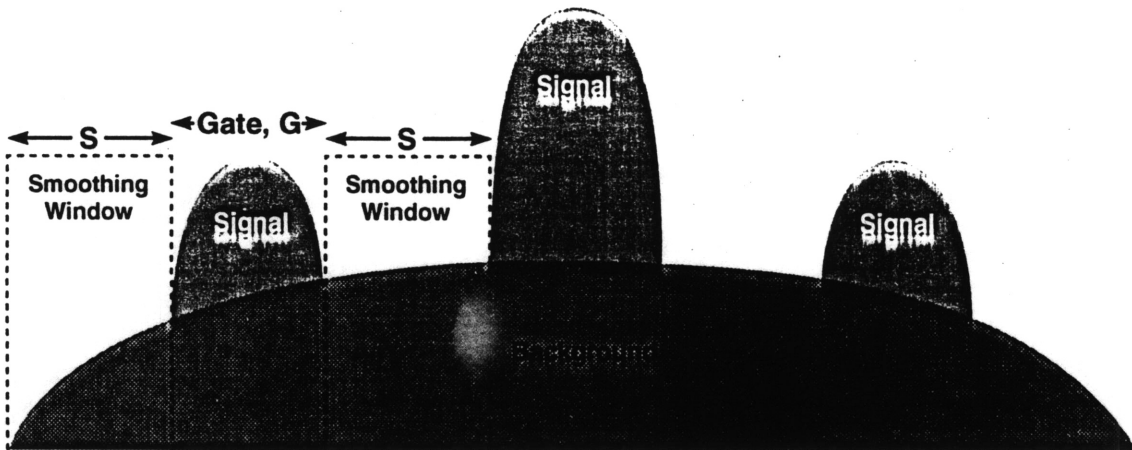


Figure 8-1: Noise Spectral Equalizer

and replacing  $z_i$  with the average  $\bar{z}_i$  if  $z_i$  is greater than  $c\bar{z}_i$  where  $c$  is a clipping constant. Smoothing the spectrum is similar to the clipping algorithm with  $c = 0$  so that all of the bins are replaced with averages, effectively low-pass filtering the spectrum. The three-pass NSE is a time-tested, simple, but effective method which provides a useful estimate of the background PSD. The first two passes utilize the clipping algorithm, and the final pass smooths the spectrum. The result is a background noise estimate which is typically divided into the signal to normalize the noise to mean 1, which can then easily be subtracted. Then a perfect background estimate ( $\mu_k^m$ ) would yield after subtraction

$$E \left\{ \frac{z_k^m}{\mu_k^m} - 1 \right\} = \frac{s_k^m + \mu_k^m}{\mu_k^m} - 1 = \frac{s_k^m}{\mu_k^m} = \bar{s}_k^m, \quad (8.2)$$

an estimate of the single-bin SNR. Many algorithms use the same three-pass template, just different  $S, G$  and  $c$  parameters that are intended to *optimize* the algorithm for a particular application. Two published examples of parameters developed for the NSE template are Real-Time Signal Processing (RTSP) and TX.

In total then, there are seven parameters which can be altered for the three-pass split-windowed NSE: two thresholds ( $c$ ), two gap widths ( $G$ ) and three smoothing

window lengths (S).

## 8.2 Optimizing the Three-Pass NSE

Our example will consist of a simplified data plus background signal to help gain an intuitive notion for what parameters will optimize the NSE. After gaining that intuition, this thesis will demonstrate its validity using a complex synthetic signal and a synthetic background.

The NSE creates a background estimate and then normalizes the original scan with the estimate. We will look to minimize the mean-square error (MSE) between the background estimate ( $\hat{\mu}_k^m$ ) and the original background ( $\mu_k^m$ ),

$$\text{MSE} = \sum_I (\hat{\mu}_k^m - \mu_k^m)^2, \quad (8.3)$$

which, in turn, will reconstruct the signal by removing much of the background noise. One way to do this reliably is to first generate the scan by adding a background spectrum to a signal spectrum, run the NSE on the resulting spectrum and compare the background estimate with the original background.

First off, it is important to note that optimizing the NSE is a difficult procedure due to the heavy correlation between some of the parameters. We will show that the optimal smoothing and gate parameters are functions of the signal shape, but also that they rely heavily on each other. For example, if we find the optimal gate parameter and then proceed to optimize the smoothing window lengths, we could very well find a new optimal gate width for the optimized smoothing window lengths. This process could go on ad infinitum, but this thesis attempts rather to develop an intuitive sense of what parameters minimize the MSE of the background estimate.

### 8.2.1 Optimal Gate Width

The synthetic signal and background used for this analysis is the model of Figure 4-4 with  $M = 10$ ,  $K = 10$ ,  $I = 265$  and  $a = 2$ . Equation 8.3 is plotted in Figure 8-2 for



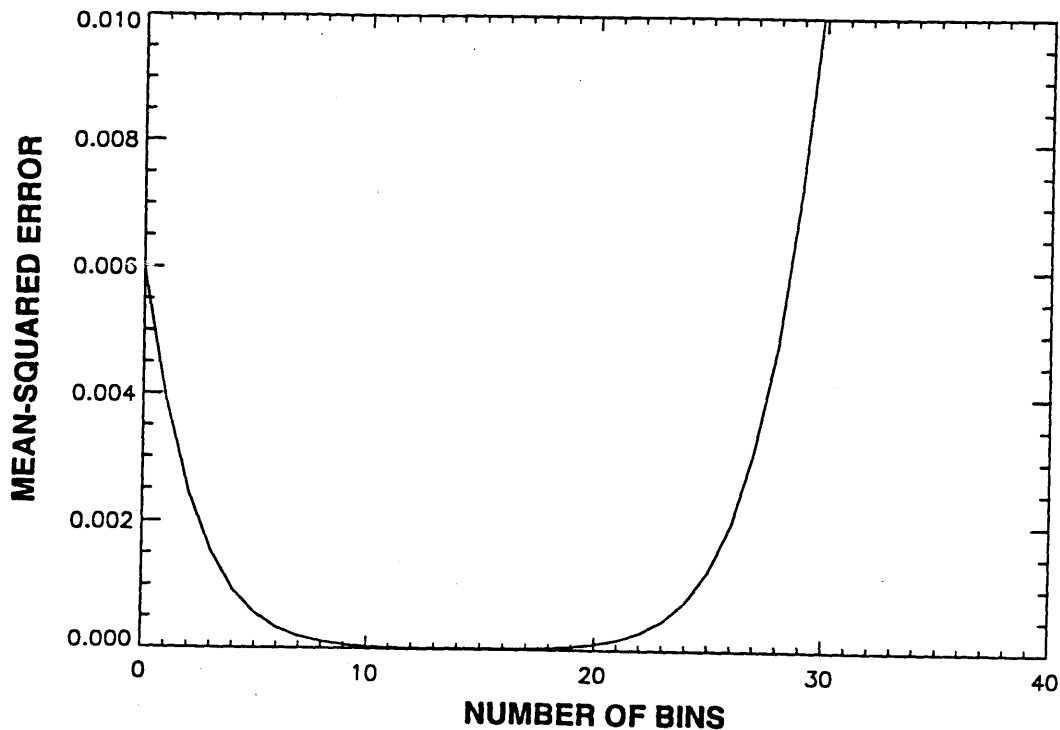


Figure 8-2: MSE vs. Gate Width

this synthetic signal model with varying first gate width ( $G_1$ ) and fixed other NSE variables.

Essentially the same problem occurs if the gate width is either too wide or too narrow; the problem is signal contamination. A narrow gate will allow the window averages to include parts of the signal feature, thereby raising the average for which the bin of interest is thresholded against. If this threshold increases due to signal contamination, some signal-containing bins may not be clipped and will then be considered background, increasing the MSE of the background estimate. If the gate is too wide, the smoothing windows may include signal bins from the adjacent feature regions in the background average. This inflated average results in the same MSE increase that stems from narrow gate widths. Considering these trade-offs, one wants the gate width to be approximately the bandwidth of the widest signal feature (Figure 8-3). This way, the NSE will compare all the bins of the widest feature against a smoothing window average that contains only background from either side of the feature region rather than signal from the feature region itself. If there are large

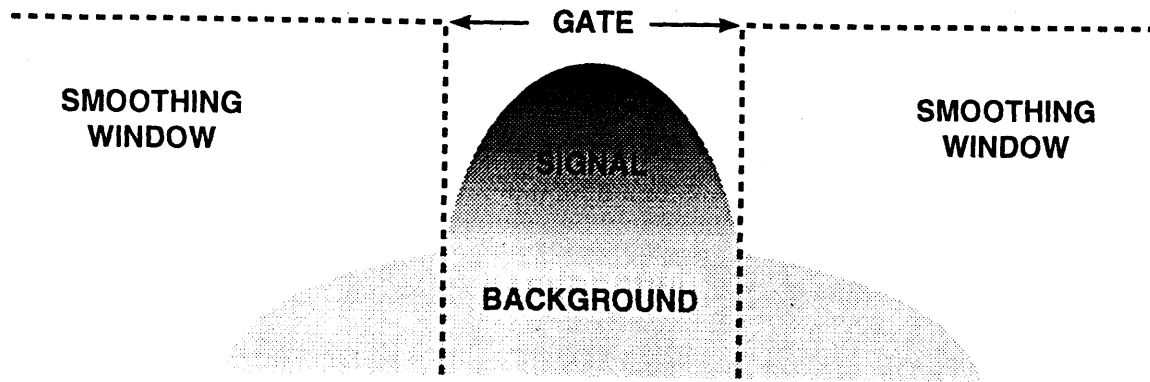


Figure 8-3: Optimal Gate Width Over Largest Feature

amounts of space between the signal features, one can exploit this by increasing the width of the gate in an effort to flatten the signal feature even more when creating the background estimate.

The optimal gate size for the second pass follows similar reasoning as to the optimal gate size for the first pass. We want to avoid signal contamination from feature regions in the smoothing window averages in order to optimize the background estimate. Figure 8-4 demonstrates how the first pass is most effective at removing the center of the signal feature, leaving signal to be clipped at the edges of the feature on the second pass of the NSE.

Running the same simulation with a varying second gate width ( $G_2$ ) demonstrated that the optimal second gate width follows roughly the same optimality criterion as the first.

## 8.2.2 Optimal Smoothing Window Length

The smoothing windows provide an estimate of the background present in the signal feature region. This enables us to replace the clipped signal bin with an estimate of the background contained in that bin. For relatively flat backgrounds the longer the smoothing window the less the variance of the sampled average and a better resulting background estimate. In this case, the limiting factor is the distance to the

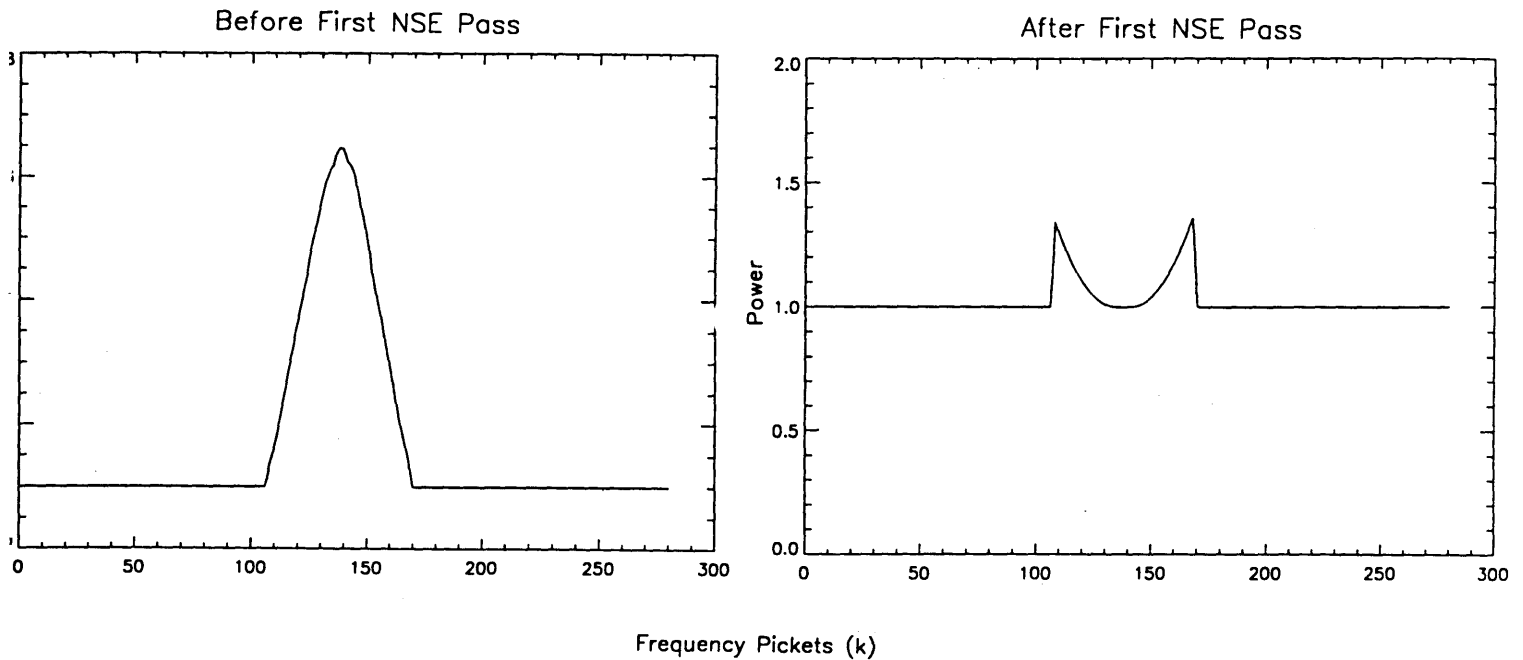


Figure 8-4: First pass clipping effect on signal feature

nearest adjacent background feature region. For complex backgrounds however, a more localized average will give a better estimate of the background for that region of the frequency spectrum. Specifically, the window can be no wider than the bandwidth over which the background mean is nominally constant.

Smoothing window lengths should increase in size for every pass to minimize the mean-square estimation error. The initial smoothing length should be approximately the smallest space between features in order to avoid contamination to the average from other signal features. This again is intimately related to the width of the gate (i.e. the wider the gate, the shorter the smoothing window and vice-versa.)

The second pass smoothing length is optimized when its value is somewhere between the length of the first pass and the length of the third. Figure 8-5 shows that the MSE is relatively similar for these values, but increases when either smaller or larger than approximately 10 bins. The wiggles in Figure 8-5 are a result of the expanding smoothing window absorbing signal features that bias the average up (increasing the MSE) and expanding over background-only bins that lower the average (decreasing

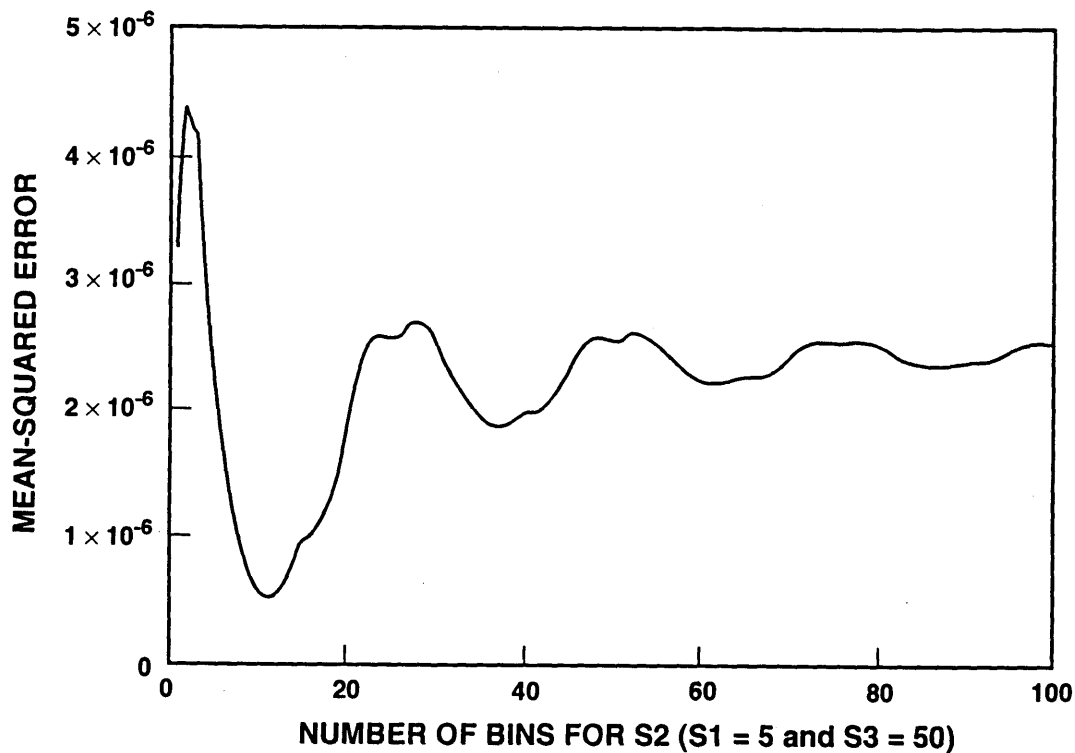


Figure 8-5: Second Pass Window Length vs. MSE

the MSE).

The final pass should be the longest smoothing window. For a perfectly flat background spectrum (i.e. white noise), the optimal third pass is a smoothing window the length of the entire spectrum. However, assuming some deviations from strictly white noise occur in the background spectrum, the estimation should use a smoothing window length at most the length between the two closest background features.

### 8.2.3 Optimal Threshold

The ratio of the center gate picket to the smoothing window average is compared to a threshold to determine whether or not to be clipped. For the more benign backgrounds, a threshold close to 1.0 will best separate the signal from background. However, as the background features become more prevalent, we must raise the threshold value in order to avoid clipping background features from the background estimate. The optimum threshold increases proportionately as the background spectrum be-

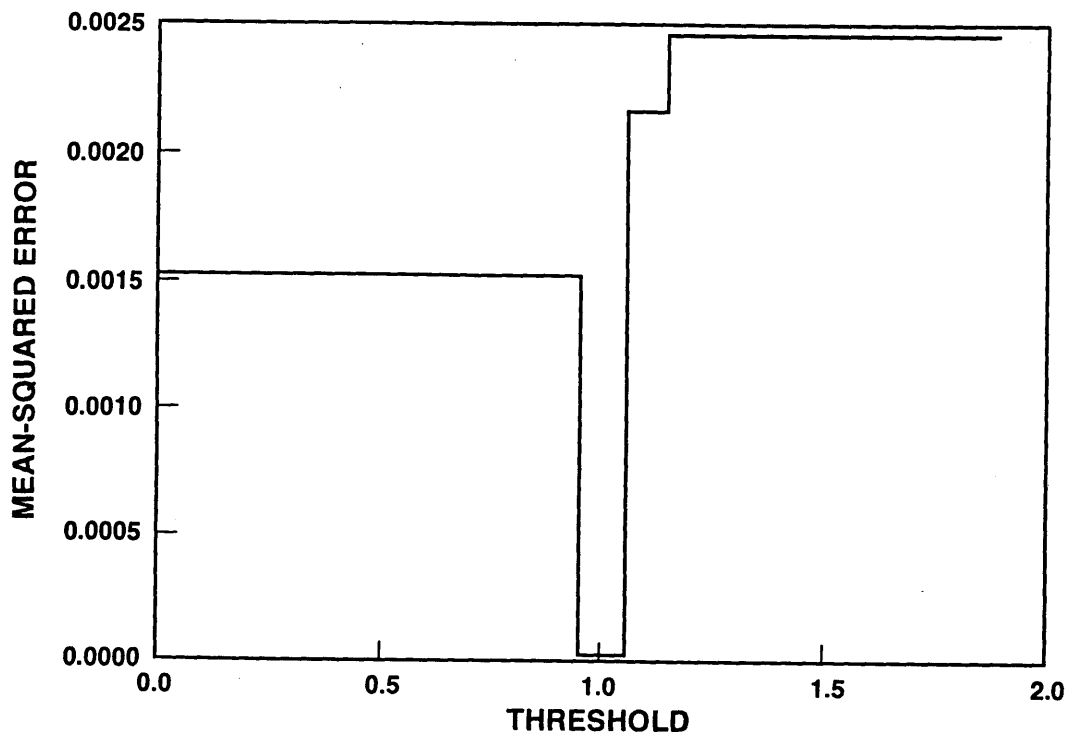


Figure 8-6: Optimal Threshold for Flat Background and Low SNR

comes less quiescent. Chapter 9 will demonstrate how threshold values greater than one yield more accurate background estimates in the non-quiescent scenarios.

In Figure 8-6 there is a very obvious choice for the optimal threshold value. However, Figures 8-7 and 8-8 depict a wider selection of optimal threshold values at higher signal-to-noise ratios.

At higher signal-to-noise ratios, when the signal exceeds the background level by twice the energy or more, raising the threshold value does not affect the background estimator. This is because the signal still exceeds the local bin average multiplied by threshold constants larger than one.

Also at high signal-to-noise ratios, lowering the threshold below one will not affect the background estimation (note Figure 8-8.) The feature regions will far exceed the local background averages and will be clipped from the background estimate. The biggest concern with lowering the threshold is that background features will begin to exceed the local averages and be clipped from the estimate. However, at high SNRs,

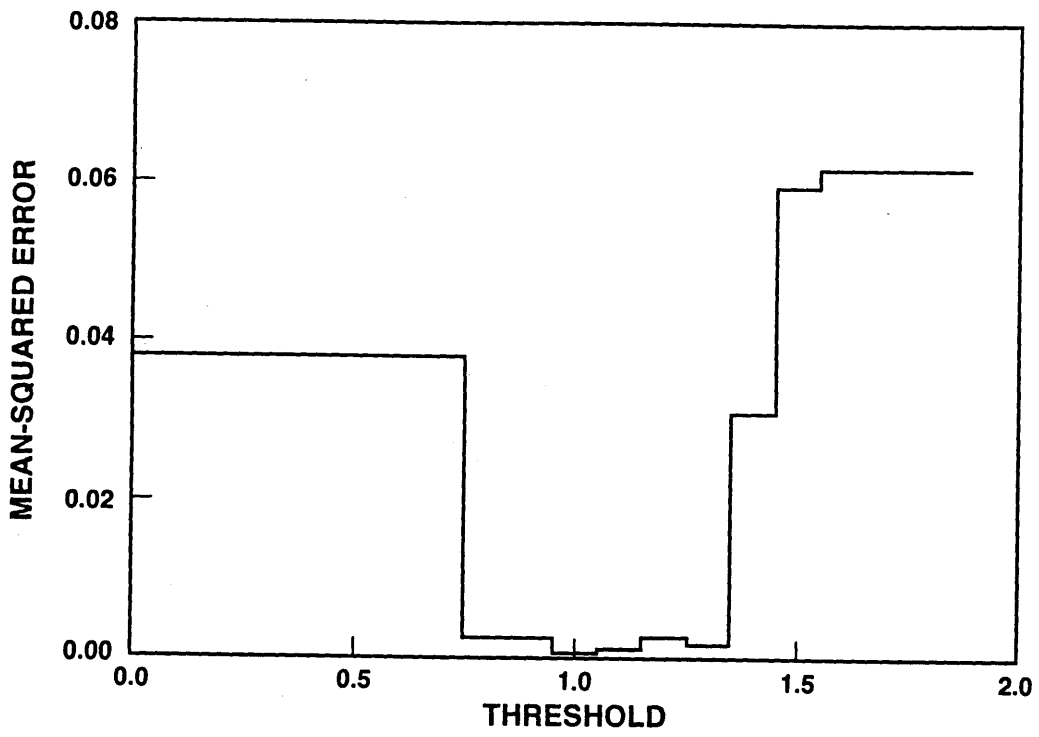


Figure 8-7: Optimal Threshold for Flat Background and Mid SNR

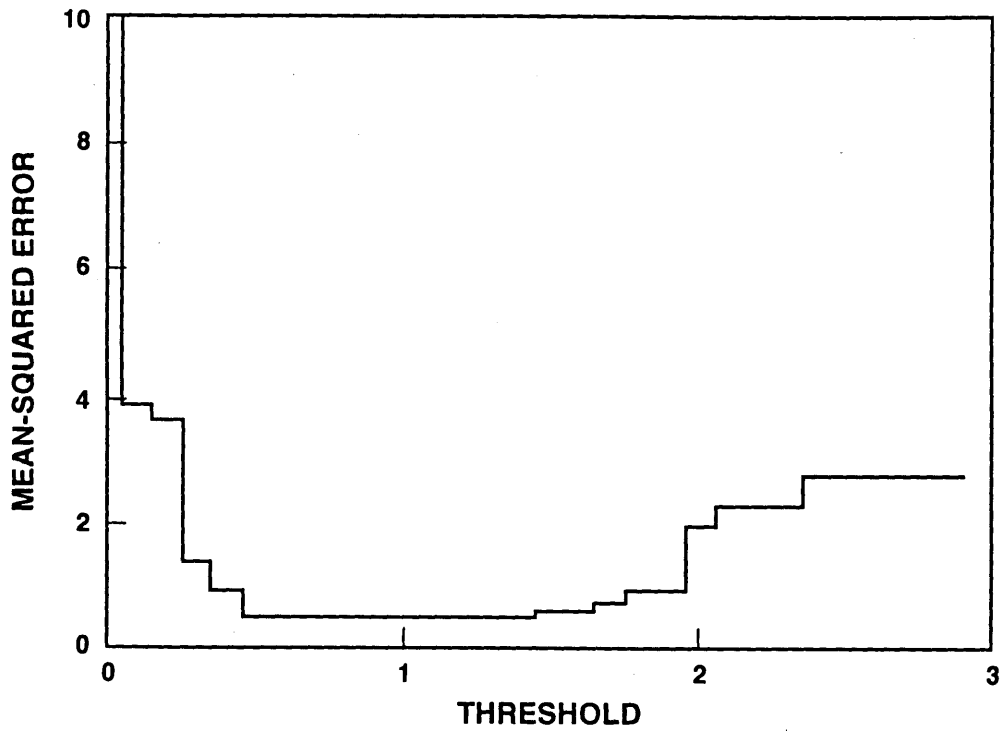


Figure 8-8: Optimal Threshold for Flat Background and High SNR

the background features will be thresholded against signal contaminated averages large enough so that even fractional thresholds will not be exceeded by background features.

#### **8.2.4 NSE Parameter Setting Summary**

- Gate widths should be at least as large as largest signal feature, any bit larger will reduce the optimum smoothing window size.
- First smoothing window should be no larger than smallest space between signal features.
- Subsequent smoothing windows should increase in size depending on the flatness of the background.
- The final smoothing window is optimized when its length is the shortest distance between two background features.
- Threshold should be close to 1.0 for featureless backgrounds, and proportionately larger for heavily featured backgrounds.



	$G_1$	$G_2$	$S_1$	$S_2$	$S_3$	$T_1$	$T_2$
ONSE	150	150	37	105	205	1.0	1.0
TX	25	25	8	25	64	1.4	1.4
RTSP	3	3	32	16	16	1.7	1.6

Table 8.1: Three-Pass NSE Parameters

### 8.3 Comparison of NSE Parameters

As shown in the previous section, NSE parameters can be developed which optimize background estimates from data collected for a specific template in a specific background environment. Typically a more robust estimator is required, one which gives a little in optimization for a particular situation in order to become a better estimator under other circumstances.

Using the guidelines developed in this chapter, we constructed an optimal NSE (ONSE) for a particular synthetic signal and white noise. Table 8.1 lists the two gate widths ( $G_1, G_2$ ), three smoothing window lengths ( $S_1, S_2, S_3$ ), and the two thresholds ( $T_1, T_2$ ).

The relative performance of these parameters is compared in Chapter 9 for real and synthetic signals and background noise.

# Chapter 9

## Evaluation of Background Estimators

Background estimators differ widely, both in their construction and their ability to construct an accurate estimate. The difficulty lies in the radically different background scenarios one can experience in the ocean (section 4.1). One estimator may minimize the mean-square error and give the highest probability of detection using the GLRT under one scenario, while failing miserably and being among the worst of the background estimators under other conditions.

### 9.1 Data Generation

This chapter presents LRT constructed boundaries for different combinations of real and synthetic target data and real and synthetic background noise. The synthetic target data includes broadband, midband and narrowband signals, although we are only concerned with midband sized features in this particular example. The real data not only includes the different sized features, but naturally has background noise included as well. In order to try and separate the real signal from its inclusive noise we use a background estimator (ONSE) to estimate the background and normalize the signal. Although this result will not resolve exactly which parts of the real data are signal and which are background noise, it gives a good approximation of the

real signal. The synthetic background noise is a synthesized benign or quiescent background environment, best described as “white noise”. The real background data is a particularly harsh background that includes clutter. The simulation results show the huge differences in choice of background estimators for a given background environment.

In this Chapter’s performance analysis ROC plots, the PLSNR was adjusted for each plot to achieve a performance point of  $(P_F, P_D) \simeq (10^{-3}, 0.9)$  for the best performing background estimator given a certain input. The process was run using the GLRT outlined in this thesis with  $N = 10$  time epochs and a total number of trials of  $10^4$ . This gave us 10 threshold values upon which to create a statistically significant threshold for our  $P_F = 10^{-3}$ . Figure 4-2 is an ASCAN of the synthetic signal being used for this chapter<sup>1</sup>. The gram and ASCAN of the synthetic and real background used for this chapter’s analysis are pictured in Figures 4-7 and 4-8 respectively. The synthetic signal is injected into the background noise by means of adding the two time series. Because of the necessary processing of the real signal, we add the processed real signal gram to the background grams.

## 9.2 Detector Performance Results

First, we look at the simulation results for a synthetic signal injected into a synthetic background (Figure 9-1). This plot includes a *known-background* result which consists of taking the white noise average and using it as a background estimate. The known estimate results in superior performance, unfortunately prior knowledge of the background is not applicable to real-life scenarios. Note that the next best results are for the ONSE which was developed using the guidelines from Chapter 8 to optimize performance for this particular synthetic model and background. The next most successful simulation result was that of TX, and RTSP had the worst performance on this particular test. Examining the table of NSE parameters it is evident that in the white noise case the wider gap widths and wider smoothing windows benefit the

---

<sup>1</sup>The unprocessed real signal provides no insight and so is not shown.

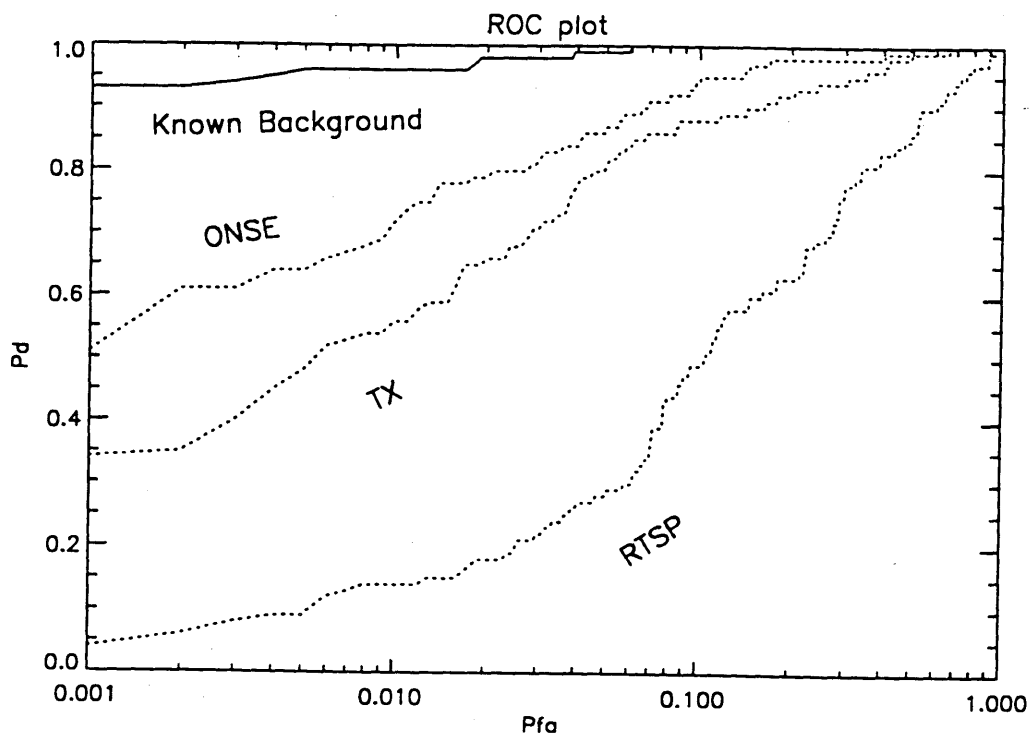


Figure 9-1: Synthetic Signal and Synthetic Background, PLSNR = -23.42dB

background estimation and hence the detector performance.

When we look at the results of injecting the synthetic signal into the real background (Figure 9-2) we can see the drastic affect it had on the ONSE background estimator. This is understandable since the ONSE contains large smoothing windows which will contribute a higher average to the clipped bins (recall  $T_1 = T_2 = 1.0$ ) because of the strong signal-like clutter. RTSP performs almost as well as the TX background estimate, but it does suffer at low  $P_F$  values. This occurs because of the largest half-dozen threshold values computed under the  $H_0$  case for RTSP far exceed the other threshold values. This can be explained if one considers the shortness of the RTSP smoothing windows. If RTSP clips narrowband background clutter in a signal region and replaces it with the smoothing average, the smoothing average will have a greater variance than the smoothing variances for the longer smoothing windows of the ONSE and TX background estimates. This greater variance in smoothing values causes a correspondingly larger variance in the LRT results under  $H_0$  in the instances where this narrowband signal-like clutter appears. This process ultimately leads to

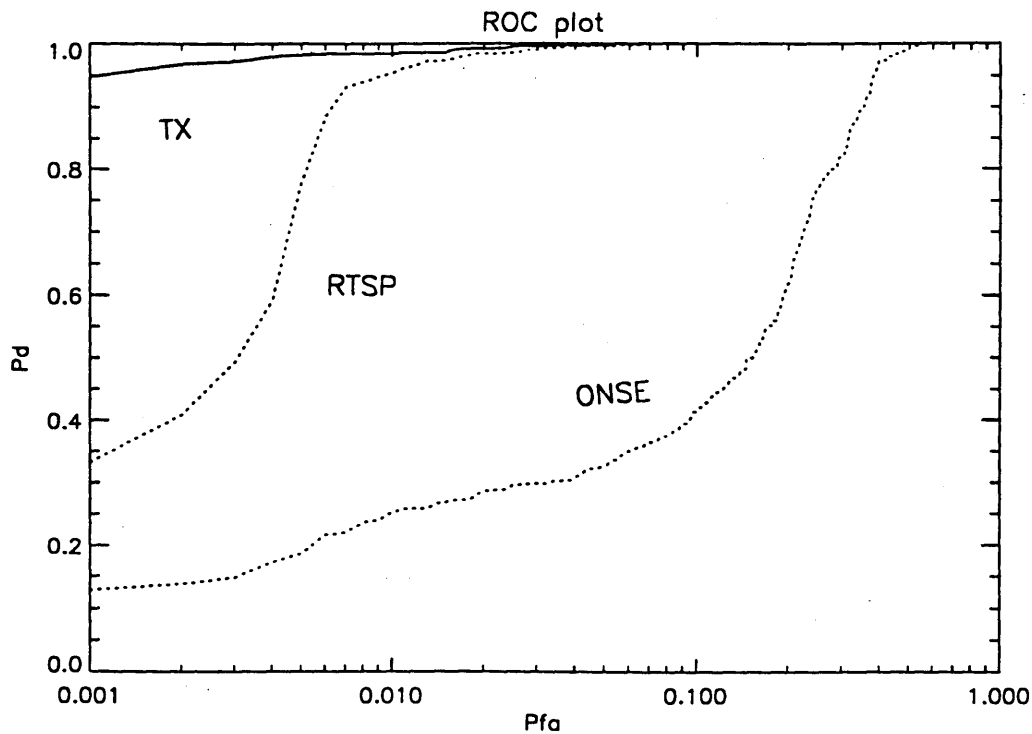


Figure 9-2: Synthetic Signal and Real Background, PLSNR =  $-11.69\text{dB}$

the difficulty RTSP has with low  $P_F$  values for this particular simulation.

The long smoothing windows of the ONSE background estimator allow its performance to exceed that of RTSP and TX for the case with synthetic background and real signal (Figure 9-3). There is no signal-like clutter to worry about in this white noise environment, so the longer the averaging over the background, the less the variance and the better the performance.

Finally, in Figure 9-4, we see how truly damaging optimizing a NSE for a particular background (ONSE) can be when used on different backgrounds. In this case, the ONSE background estimator is clipping much of the background clutter and considering it signal, while RTSP is smoothing out all of the clutter (and some of the signal.)

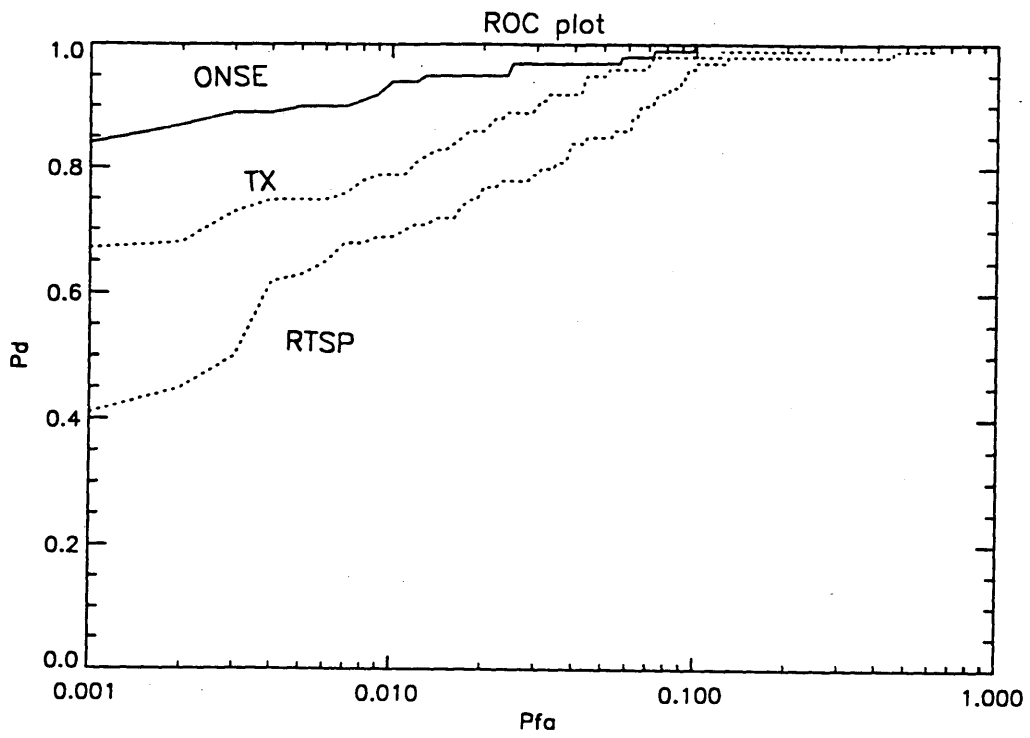


Figure 9-3: Real Signal and Synthetic Background

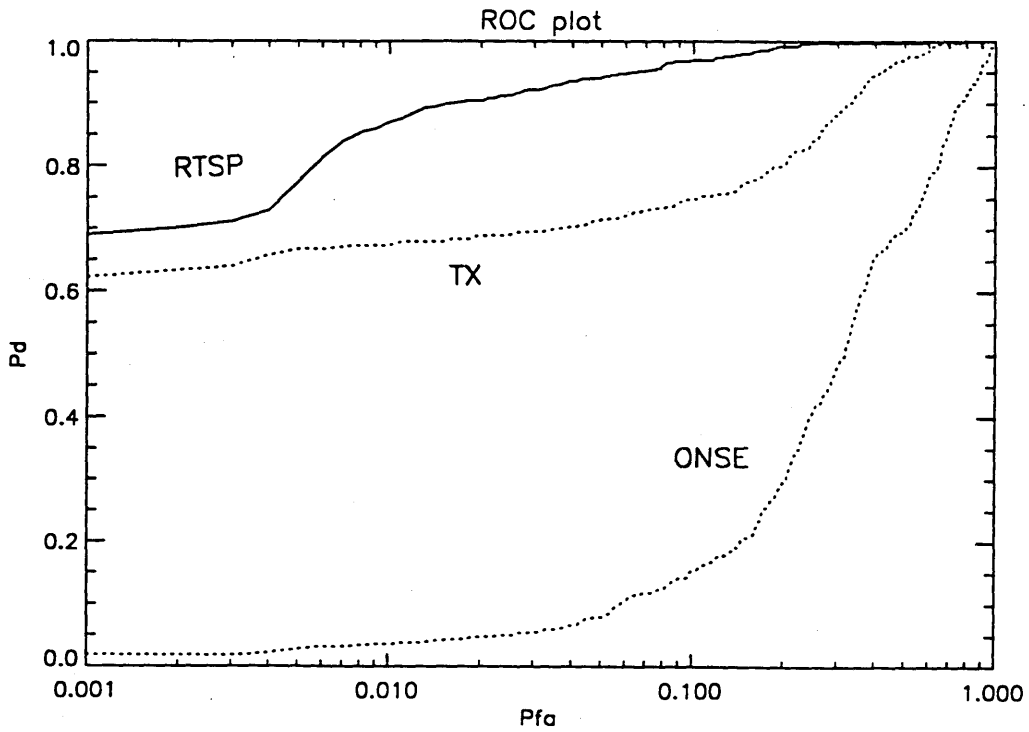


Figure 9-4: Real Signal and Real Background

# Chapter 10

## Conclusions

This thesis began with a theoretical and experimental analysis of the single-bin statistical nature of ocean acoustic data. We concluded that Gaussian time-series assumptions captured the essential features of a wide range of ocean acoustic data. Chapter 3 introduced the theory behind target detection and the LRT optimal detector. Using our knowledge of the single-bin statistics, Chapter 4 developed models for the signal and background noise environment. We analyzed both simple “boxcar” models and more complex models that better represented real signal and background spectrums. Using this modeling information we were then able to develop a LRT that enabled us to compute the “optimal” detection performance for known-input scenarios and then a Generalized LRT that enabled us to explore the performance of background estimators. Next we developed several signal-to-noise ratio definitions which enabled us to measure not only the relative strength of background and signals, but gave us insight into the performance of detectors given a certain input data set. Using synthetic models we explored the validity of Chernoff performance approximations and the remarkably similar error-function approximation computations as compared to the simulated LRT process. Chapter 7 analyzed the LRT and a few other more practical detectors in a closed form analysis so that we gain insight into the benefits and drawbacks of detector choices and their relation to performance. The next step was to introduce a popular background estimation technique with variable parameters, and to develop guidelines by which this estimation technique can best be optimized

for given background noise and signal inputs. Finally, Chapter 9 allowed us to pool the results of much of this thesis into simulations, using real and synthetic data, that contributed insight into how these detection tools worked and lent validity to our previous assumptions.

Many tenets of this thesis only touch on ideas that have not been fully explored. For instance, optimizing background estimators is a project of overwhelming proportions. This thesis developed a background estimator that retained a fixed shape for each pass. Performance may be improved if we could optimize the background filter for each bin of every feature region, taking advantage of the narrowest possible gate width and the longest smoothing window.

Another issue that could be further explored is that of detector performance. The closed form analysis of Chapter 7 only analyzed three detectors for simplified signals, much insight could be gained from exploring more complex models and other detectors.



# Appendix A

## Exponential Bin Statistics

### Derivation

This appendix provides a mathematical explanation for the statistically exponential output of the magnitude-square transform outlined in chapter 2.

Let  $\underline{X}_n = a + bj$  be the complex output of the FFT (see Figure 2-1) where  $a = \Re\{\underline{X}_n\}$  and  $b = \Im\{\underline{X}_n\}$ . By definition, the magnitude-square of a complex variable is the sum of the squares of the magnitudes,

$$|\underline{X}_n|^2 = |a + bj|^2 = |a|^2 + |b|^2 = a^2 + b^2 = \zeta. \quad (\text{A.1})$$

Now the probability distribution function for the system output (again in reference to Figure 2-1),  $z_{nk}$ , can be written as

$$P_\zeta(z_{nk}) = Pr(\zeta \leq z_{nk}) = Pr(a^2 + b^2 \leq z_{nk}) = \int_0^{\sqrt{z_{nk}}} da \int_0^{\sqrt{z_{nk}-a^2}} db p_{a,b}(a, b). \quad (\text{A.2})$$

The joint probability density function (PDF) of  $a$  and  $b$ , where  $a$  and  $b$  are independent, identical and normally distributed with zero mean and variance  $\sigma^2$  is defined as

$$p_{a,b}(a, b) = p_a(a)p_b(b) = \frac{e^{-\frac{a^2}{2\sigma^2}}}{\sqrt{2\pi\sigma^2}} \frac{e^{-\frac{b^2}{2\sigma^2}}}{\sqrt{2\pi\sigma^2}} = \frac{e^{-\frac{(a^2+b^2)}{2\sigma^2}}}{2\pi\sigma^2}. \quad (\text{A.3})$$

Now Equation A.2 becomes,

$$P_{\zeta}(z_{nk}) = \int_0^{\sqrt{z_{nk}}} da \int_0^{\sqrt{z_{nk}-a^2}} db \frac{e^{-\frac{(a^2+b^2)}{2\sigma^2}}}{2\pi\sigma^2}. \quad (\text{A.4})$$

Using polar notation we can define  $R = \sqrt{a^2 + b^2}$ ,  $\phi = \arctan(\frac{b}{a})$  and  $dadb = RdRd\phi$ , so we can write Equation A.4 as an integral over a circle with radius  $R$

$$Pr(\zeta \leq z_{nk}) = Pr(R \leq \sqrt{z_{nk}}) = \int_0^{\sqrt{z_{nk}}} RdR \int_0^{2\pi} \frac{e^{-\frac{R^2}{2\sigma^2}}}{2\pi\sigma^2} d\phi \quad (\text{A.5})$$

$$\begin{aligned} &= \int_0^{\sqrt{z_{nk}}} dR \frac{R}{\sigma^2} e^{-\frac{R^2}{2\sigma^2}} \\ &= -e^{-\frac{R^2}{2\sigma^2}} \Big|_0^{\sqrt{z_{nk}}} \\ &= 1 - e^{-\frac{z_{nk}}{2\sigma^2}}. \end{aligned} \quad (\text{A.6})$$

Now we simply differentiate Equation A.6 in order to verify the PDF of the magnitude-squared Gaussian random variable,

$$p_{z_{nk}}(z_{nk}) = \frac{d}{dz_{nk}} Pr(\zeta \leq z_{nk}) = \frac{1}{2\sigma^2} e^{-\frac{z_{nk}}{2\sigma^2}} \text{ for } z_{nk} \geq 0. \quad (\text{A.7})$$

The result yields the PDF of an exponential random variable with mean  $2\sigma^2$  and variance  $4\sigma^4$  [6].

# Bibliography

- [1] Johann L. Codona. NSE and gray-scale design for full spectrum processing. Technical report, AT&T Bell Laboratories, 1973.
- [2] Thomas J. Green, Jr. Type-I signal detection for E-systems. Lincoln Laboratory Internal Memo, 1994.
- [3] Thomas J. Green, Jr. Background estimation in the presence of narrowband acoustic signals. Lincoln Laboratory Internal Memo, 1996.
- [4] Richard O. Nielsen. *Sonar Signal Processing*. Artech House, 1991.
- [5] Alan V. Oppenheim. *Discrete-Time Signal Processing*. Prentice Hall, 1989.
- [6] Jeffrey H. Shapiro. A receiver operating characteristic relevant to broadband sonar detection. Lincoln Laboratory Internal Memo, 1994.
- [7] Jeffrey H. Shapiro. Type-I signal detection in the presence of clutter. Lincoln Laboratory Internal Memo, 1995.
- [8] Merrill Skolnik. *Radar Handbook*. McGraw-Hill Publishing Company, 1990.
- [9] Robert J. Urick. *Principles of Underwater Sound*. Peninsula Publishing, 1983.
- [10] Harry L. Van Trees. *Detection, Estimation, and Modulation Theory*. John Wiley and Sons, 1968.
- [11] Alan S. Willsky, Gregory W. Wornell, and Jeffrey H. Shapiro. Stochastic processes, detection and estimation. 6.432 Supplementary Class Notes, 1996.